

STRATIGRAPHIC EVOLUTION OF AN ESTUARINE FILL SUCCESSION, AND  
RESERVOIR CHARACTERIZATION OF INCLINED HETEROLITHIC  
STRATA, CRETACEOUS OF SOUTHERN UTAH, USA

by

Ryan Michael Purcell

A thesis submitted to the faculty of  
The University of Utah  
in partial fulfillment of the requirements for the degree of

Master of Science

in

Geology

Department of Geology and Geophysics

The University of Utah

December 2015

Copyright © Ryan Michael Purcell 2015

All Rights Reserved



## ABSTRACT

A complex mixture of wave, tide, and fluvial energies form paralic strata, and although these units are important hydrocarbon reservoirs, they are complex and poorly understood. This study documents the architecture of an estuarine succession using outcrops of the Upper Cretaceous John Henry Member of the Straight Cliffs Formation, southern Utah (USA). Terrestrial LiDAR, photomosaics, 18 detailed measured sections, and 652 paleocurrent indicator measurements inform this stratigraphic analysis. The ~65-m-thick interval of interest records evolution of a mixed-energy to wave-dominated estuary, with basal elongate tidal bars overlain by carbonaceous bay fill, tidal flat deposits, a bayhead delta, and ultimately a coastal plain succession.

A detailed interpretation of the ~8.5-m-thick by 550-m-wide bayhead delta outcrop highlights internal architecture as well as the relationship between the bayhead delta, the underlying tidal bar units, and the overlying coastal plain strata. Within the bayhead delta, beds are composed of very fine- to medium-grained trough cross-stratified, rippled (some climbing), planar laminated, planar cross-stratified sandstones, and interbedded mudstone/siltstone. These units thicken and coarsen vertically. Statistical analysis of the bayhead delta indicates that average bedding thickness, net to gross, amalgamation ratio and grain size increase down-dip, and vertically up-section. This study compares grain size analysis results to a published study of a heterolithic fluvial point bar to provide guidelines for subsurface differentiation of inclined heterolithic strata, and to better

predict the impact on reservoir distribution and probable fluid flow pathways.

Understanding the variety of expressions and reservoir behavior of IHS intervals will guide future studies of heterogeneous paralic reservoirs.

## TABLE OF CONTENTS

ABSTRACT.....	iii
LIST OF FIGURES.....	vi
ACKNOWLEDGEMENTS.....	viii
INTRODUCTION.....	1
GEOLOGIC BACKGROUND AND PREVIOUS WORK.....	6
METHODS.....	12
RESULTS.....	18
Paralic Environment Facies Analysis.....	18
Analysis of Spatial Data from the Bayhead Delta Reservoir Analog.....	30
DISCUSSION.....	59
Bayhead Delta IHS Characterization.....	59
Tibbet Canyon Estuarine Evolution.....	63
Stratigraphic Correlations.....	66
CONCLUSIONS.....	80
REFERENCES.....	82

## LIST OF FIGURES

Figure	Page
1. Map of the Kaiparowits Plateau of southern Utah.....	8
2. Regional stratigraphy of the Kaiparowits Plateau and detailed stratigraphy of the Straight Cliffs Formation.....	10
3. Tibbet Canyon study area location map.....	14
4. LiDAR outcrop interpretation of Tibbet Canyon RPTC-2.....	16
5. Facies hierarchy.....	35
6. Bayhead delta bedding hierarchy.....	37
7. Estuary fill facies.....	42
8. Bayhead delta facies.....	44
9. Bayhead delta outcrop interpretation.....	46
10. Tide-influenced coastal plain facies .....	48
11. Coastal plain facies.....	50
12. Bayhead delta measured section correlation.....	52
13. Lateral outcrop statistical trends.....	55
14. Vertical grain size trends.....	57
15. Bayhead delta outcrop model.....	72
16. Grain size proportion curve comparison of a bayhead delta and tidally influenced point bar.....	74
17. Depositional model and estuary evolution of Tibbet Canyon strata	

	at RPTC-2.....	76
18.	Southern Kaiparowits Plateau stratigraphic correlation .....	78



## ACKNOWLEDGEMENTS

I would like to thank my advisor, Dr. Cari Johnson, for her support and guidance throughout this project. Also, special thanks to Dr. Lisa Stright and Laruen Birgenheier for participating in this process as members of my thesis committee. Thanks to all those who assisted me as field assistants: Brenton Chentnik, Kyle Mika, David Wheatley, Jon Primm, and Will Gallin. Thanks to Penn State student Ellen Chamberlin for her help and expertise with terrestrial LiDAR. This project was made possible by support through the University of Utah Rock to Models research group by Chevron, ConocoPhillips, Hess, Shell, and Statoil. Thanks to the Bureau of Land Management and the Grand Staircase-Escalante National Monument for granting me permission to conduct research on federal land. Finally, I am grateful to all my family, friends, and the University of Utah Geology Department who have supported me and made this possible.

## INTRODUCTION

Despite recent advancements in understanding paralic depositional environments, documentation concerning the nature of these deposits is still lacking. Paralic environments occur at or near sea level and include deltas, shoreline-shelf systems, and estuaries (Reynolds, 2005). These systems are notably complicated, because they represent a spectrum of fluvial, tidal, wave, and storm influences, with lateral and vertical variability at all scales. However, despite the complexity of processes forming paralic environments, facies models tend to deal mainly with end-member scenarios (Coleman and Wright, 1975; Galloway, 1975; Boyd et al., 1992, 2006; Bhattacharya, 2006), and are commonly simple and descriptive rather than predictive (Ainsworth et al., 2011). Studies of modern and ancient paralic systems (Dalrymple and Choi, 2007; Yang et al., 2005; Bhattacharya and Giosan, 2003; Willis, 2005; Yoshida et al., 2007; Ainsworth et al., 2008) have begun to recognize and incorporate mixed process factors into their models. Ainsworth et al. (2011) developed a classification scheme for clastic shorelines based on the relative dominance of wave, tidal, and fluvial processes, and incorporated it into a set of matrices and decision trees that characterize the relative impacts of different coastal processes through time and space.

Estuaries are of particular interest in the Ainsworth et al. (2011) classification scheme due to the additional complexity that embayed coastal morphologies contribute to depositional architectures. Estuaries contain both transgressive and regressive fill

(Dalrymple, 2006; Dalrymple et al., 1992), and display a tripartite geomorphology, reflecting varying degrees of relative wave, tidal, and fluvial energy (Dalrymple et al., 2012). Wave and tidal processes control the basic morphology of estuaries, and thus represent two main morphologic categories (wave- and tide-dominated). Fluvial processes mainly control the sediment flux entering the upstream portion of the estuary and do not have a significant impact on the fundamental morphology of the estuary itself (Boyd et al., 2006). Estuaries are highly complex, so in order for coastal models to become more robust, outcrop studies recording process-regime changes in these paralic environments are critical (Martinius et al., 2005).

In addition to their importance in understanding coastal processes, paralic reservoirs account for an increasingly significant portion of petroleum reserves (Terzuoli and Walker, 1997; Martinus et al., 2001; Dreyer et al., 2005; Cummings et al., 2006; Tänavsuu-Milkeviciene et al., 2009; Feldman et al., 2013, 2014). Paralic reservoirs pose a production challenge due to their heterogeneous nature. Tidal strata can be particularly heterolithic, with fine-grained, low permeability layers deposited between porous and permeable sands, typically during neap tides when current velocities are low (Visser, 1980; Burton and Wood, 2011; Dalrymple and Choi, 2007). This heterogeneity ranges from field to reservoir to bed and grain scales (Hassanpour et al., 2013). Given the three-dimensional complexities that heterogeneities create, predictive, reservoir-scale, outcrop-derived facies models are invaluable for predicting petroleum production, developing a field, and evaluating economic potential (White et al., 2004).

A particular example of problematic reservoir-scale heterogeneity is inclined heterolithic strata (IHS) (Thomas et al., 1987). The term IHS does not refer specifically to

any one type of architectural element or depositional environment, only to a recognizable arrangement of inclined, interbedded, fine- and coarser-grained facies. Some of the most noteworthy examples of IHS deposits are the tide-influenced point bars of the McMurray Formation. These deposits have garnered considerable attention because they form the best reservoir sandstones of the Alberta (Canada) Oil Sands, which are collectively one of the largest sources of *in situ* bitumen in the world (Strobl et al., 1997; Labrecque et al., 2011). These reservoirs require an extraction process called Steam Assisted Gravity Drainage (SAGD) to stimulate fluid flow (McLennan and Deutsch, 2004; Wightman, 2003; Musial et al., 2012). Permeability is one of the most important physical properties influencing hydrocarbon recovery from reservoirs, and permeability heterogeneity caused by fine-grained beds may result in barriers and baffles that hamper heat and fluid flow at multiple scales (Willis and White, 2000; Burton and Wood, 2011; Labrecque et al., 2011; Pyrcz and Deutsch, 2014). The SAGD process is intensive and costly, which necessitates a detailed understanding of the distribution of reservoir facies relative to potential barriers and baffles to flow, such as shale drapes in IHS deposits (Stobl et al., 1997; Willis and Tang, 2010; Musial et al., 2012; Fustic et al., 2013; Pranter et al., 2013).

Despite non-genetic terminology, the term IHS has become largely synonymous with tide-influenced point bar deposition, and there is a tendency to consider IHS as a tidal indicator (Choi et al., 2004). This is not surprising considering that tide-influenced environments of deposition account for the majority of published accounts of IHS (Thomas et al., 1987; Shanley et al., 1992; Gingras et al., 1999; Martinius et al., 2001; Gingras et al., 2002; Dalrymple et al., 2003; Hubbard et al., 2011; Labrecque et al., 2011; Musial et al., 2012). However, other examples of IHS exist, including deltas (Stanley and

Surdam, 1978; Steel et al., 2012; Martinius et al., 2001), meandering and mud-rich fluvial channels (Jackson, 1981; Thomas et al., 1987), and submarine fans (Miall, 1985b).

Central to the IHS interpretation issue is that there is a lack of basic conceptual models for the full range of variability of these deposits. Even within tide-influenced point bar IHS descriptions, there is controversy over the nature of mud drape deposition (Choi et al., 2004) and stratigraphic stacking relationships (Musial et al., 2012).

This study calls attention to a comparison between IHS formed by fluvial point bars versus bayhead deltas. Due to their areal extent and preservation potential, bayhead deltas can form significant economic hydrocarbon reservoirs (Hubbard et al., 2002; Terzuoli and Walker, 1997; Broger et al., 1997; Madeleine Peijs-van Hilten et al., 1998). Bayhead delta reservoirs have preserved areal extents between 9 and 100 km<sup>2</sup> and, in the Bluesky Formation of central Alberta, these reservoirs contain up to 1.5 billion barrels of oil (Hubbard et al., 2002). However, research focusing on bayhead deltas is scarce, and these units are commonly lumped in with descriptions of IHS point bars (Thomas et al., 1987; Kirschbaum and Hettinger, 2004), which they can closely resemble (Steel et al., 2012). In fact, before interpretation of the thick IHS sets of the McMurray Formation as point bars (Mossop and Flach, 1983), Carrigy (1971) recognized them as deltaic foresets, and controversy over their depositional setting and stratal evolution continues today (Musial et al., 2012). Although most studies agree that the IHS sets of the McMurray represent tide-influenced point bar deposits, the position of deposits relative to the coeval shoreline is still controversial (Carrigy, 1971; Smith et al., 2009; Musial et al., 2012; Hubbard et al., 2011).

Given the importance of paralic depositional environments in understanding the

dynamics of modern and ancient coastal processes in time and space, as well as the significant reservoir volumes that they provide for petroleum, additional outcrop studies are needed to expand existing knowledge of clastic shorelines. This study leverages excellent exposures in the Cretaceous Straight Cliffs Formation of southern Utah (USA) to understand process changes in an ancient estuarine system. Included is an account of facies architecture and evolution of the system from mixed-energy to wave-dominated. Additionally, a quantitative analysis of an IHS bayhead delta is presented to determine characteristic differences between IHS bayhead deltas and IHS point bars. Grain-size trends derived from outcrop measurements yield crucial insight into the various expressions of IHS deposits.

## GEOLOGIC BACKGROUND AND PREVIOUS WORK

This study focuses on the John Henry Member of the Upper Cretaceous Straight Cliffs Formation (Turonian–early Campanian) of the Kaiparowits Plateau, located along the western margin of the Cretaceous Western Interior Seaway (Fig. 1). The Late Cretaceous Sevier fold-thrust belt formed in response to west-east crustal shortening driven by Farallon plate subduction beneath the North America plate, which occurred from approximately Jurassic to Eocene time (Coney, 1972; Armstrong, 1968; Dickinson, 1974; DeCelles and Coogan, 2006). Crustal load-driven flexural subsidence (Currie, 2002; Jordan, 1981; Painter and Carrapa, 2013) as well as dynamic subsidence (Liu et al., 2014, 2011) led to foreland basin development east of the thrust belt. Global greenhouse climate and elevated rates of sea-floor spreading favored eustatic highstand conditions (Haq et al., 1987; Miller et al., 2005), and consequent flooding of the foreland basin formed the Western Interior Seaway (Kauffman, 1977; Hancock and Kauffman, 1979).

The Straight Cliffs Formation is composed of siliciclastic sediments derived from distributive fluvial systems draining the Sevier fold-thrust belt, Mogollon Highlands, and Cordilleran volcanic arc (Eaton, 1991; Lawton et al., 2003, 2014; Szwarc et al., in press). A northeast-flowing fluvial system, roughly axial to the Sevier fold-thrust belt in southern Utah, transported sediment to the adjacent Kaiparowits Basin (Szwarc et al., in press). Peterson (1969a, 1969b) divided the Straight Cliffs Formation into four members: the Tibbet Canyon, Smoky Hollow, John Henry, and Drip Tank Members. Outcroppings

of the Straight Cliffs Formation are accessible around the plateau, and record a broad spectrum of depositional environments, from fluvial to marginal marine. The John Henry Member is the thickest unit in the Straight Cliffs Formation (200-500 m) and has the highest degree of lateral variability. Generally, the southern and western plateau preserves fluvial and coastal plain strata (Shanley et al., 1992), and the northern and eastern plateau preserves shoreface, lagoonal, and estuarine deposits (Peterson, 1969a). Peterson (1969b) categorized marine shoreface units (A-G) which were used by subsequent studies to document stratigraphic architecture in the eastern plateau (Allen and Johnson, 2010a, 2010b, 2011; Dooling, 2013; Chentnik et al., in press) and to explain fluvial channel stacking patterns in the western plateau (Pettinga, 2013; Gooley, 2010) (Fig. 2).



Figure 1. Regional map of the Kaiparowits Plateau of southern Utah

The Straight Cliffs Formation is shaded in gray. Black dots mark previous studies of the John Henry Member. Arrows indicate the general proximal to distal facies relationships in the John Henry Member, ranging from fluvial on the western margin to marine on the eastern margin, with tidal and paralic facies in between. The red box marks the primary field location of this study (Fig. 3). Abbreviations: CNTB-Central Nevada Thrust Belt, SFTB-Sevier fold-thrust belt, WIS-Western Interior Seaway, MTB-Maria Thrust Belt. Modified from Chentnik et al. (in press).

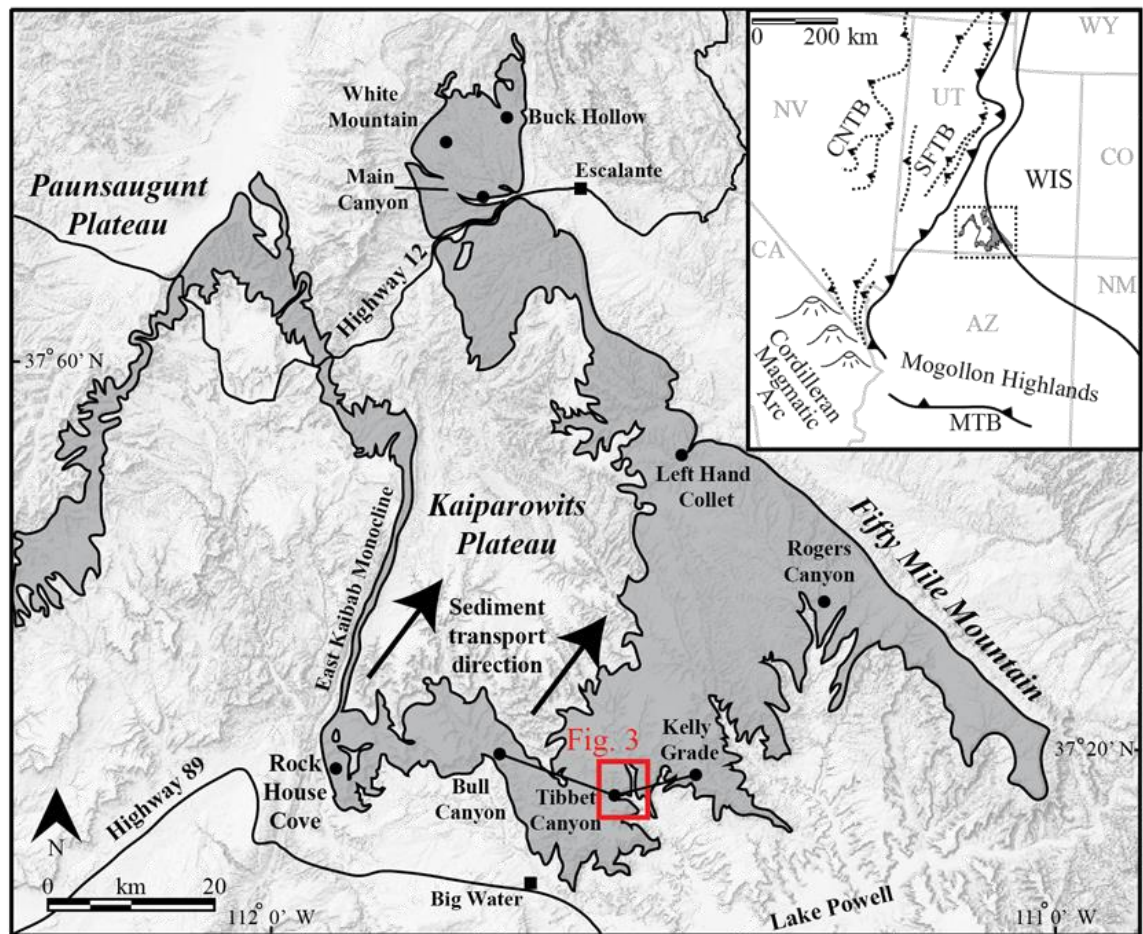
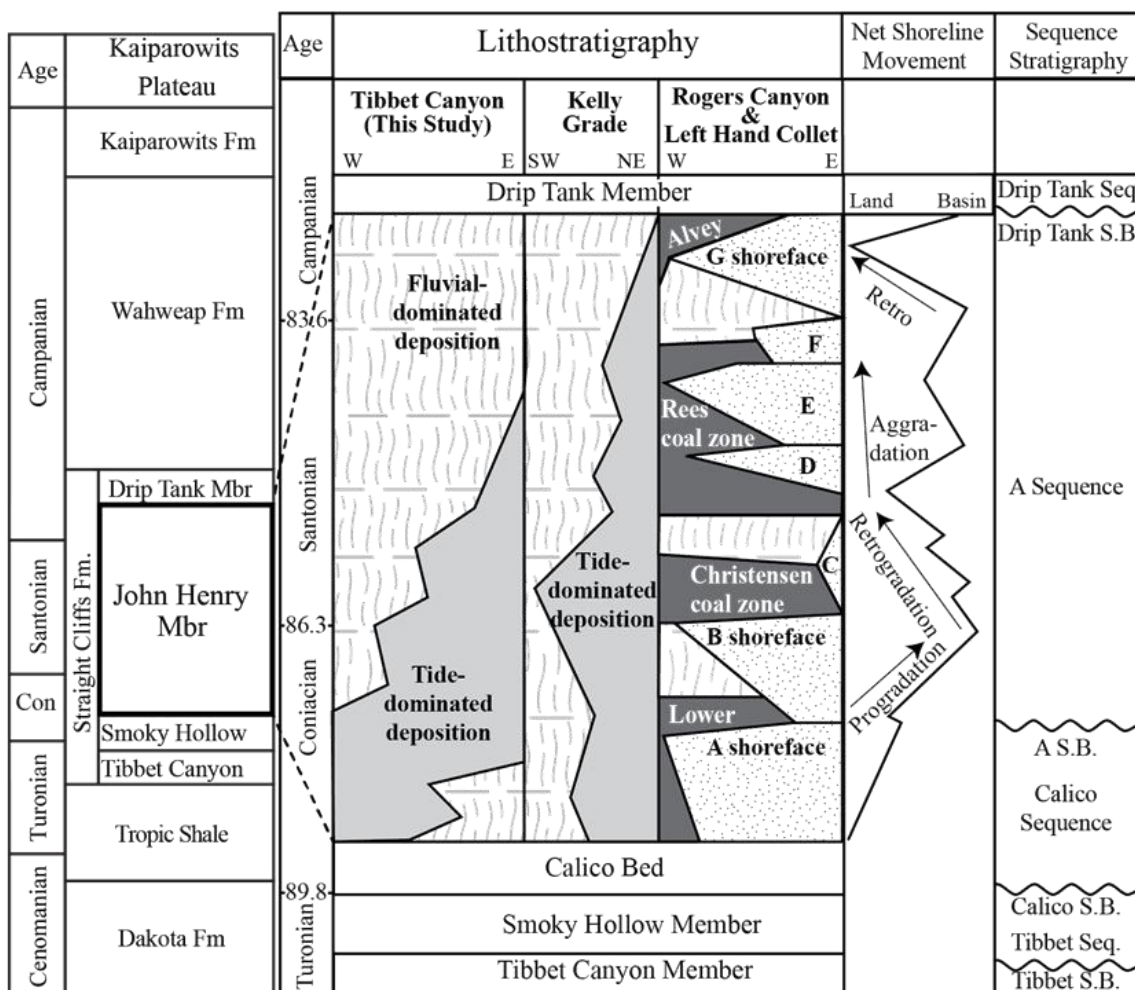


Figure 2. Regional stratigraphy

Regional stratigraphy of southern Utah including detailed stratigraphic summary chart of the Turonian-Campanian Straight Cliffs Formation, and previous lithostratigraphic and sequence stratigraphic interpretations (Shanley and McCabe, 1991). Net shoreline movement is based on shoreface pinchouts and marginal marine facies distributions at Rogers Canyon (Allen and Johnson, 2011), Left Hand Collet (Dooling, 2013) and Buck Hollow (Mulhern et al., 2014). Marine sandstone packages “A-G” are defined by Peterson (1969b) and pinch landward into coal zones and coastal plain facies. Lithostratigraphy of Kelly Grade (Gallin et al., 2010) documents relative tide- to fluvial-dominated paralic deposition.

Regional Stratigraphy

Straight Cliffs Formation, Kaiparowits Plateau



## METHODS

Five sections were measured in order to assess the facies variability within the John Henry Member in Tibbet Canyon (Fig. 3A). One general section (RPTC-2) captures the whole John Henry Member, from the top of the Calico Bed to the Drip Tank Member. Several other sections focus on the spatial variability in lower John Henry Member facies. These sections (RPTC-1, -3, -4, -5) (Fig. 3A) are measured from the top of the Calico Bed to the last appearance of IHS or to the base of purely fluvial channel deposits. Thirteen additional sections (Fig. 3B) measured at the location of RPTC-2 detail the vertical and horizontal changes of an IHS package. These sections (TCIHS-1 to TCIHS-13) (Fig. 3B) were measured from the top of the last coal layer (continuous across this outcrop) below the IHS to the top of the IHS package. The outcrop is exposed obliquely to the northeast depositional trend of the bayhead delta. Thus, moving north along the outcrop permits analysis of the bayhead delta down dip, from topset to toset, and toward the delta depositional axis (Fig. 3C). Paleocurrent indicators ( $n = 439$ ) were measured from planar-, trough-, and ripple-cross stratified sandstones, and accretion sets and bar form accretions were measured where possible ( $n = 213$ ). Terrestrial LiDAR was collected at the location of RPTC-2 (Fig. 3, Fig. 4), as well as adjacent strata within Tibbet Canyon. A 3D photorealistic version of the outcrop was created using RGB point clouds gathered from the scans, which were used as a visual aid in outcrop interpretation.

Multiple inclined surfaces were interpreted and were combined with measured

sections to serve as the basis for the bayhead delta model. A grain size well log was generated for each measured section, according to the lithology profile and description. Each measured section was then analyzed to determine amalgamation ratio, net-to-gross, and average bed thickness according to the interpreted inclined surfaces. These metrics were then compared along the length of the outcrop, from the topset to the toset of the inclined surfaces, to understand the spatial distribution of the reservoir character. A simple grid and zone model was created, constrained by the inclined surfaces interpreted in each section. Layering within each zone was set to parallel the basal inclined surfaces. Layer thickness was constrained to produce an average of 5 cm for each layer. The model contains 11 zones and 270 layers. Grain size well logs were then scaled up and sampled according to the layer increment. Finally, vertical grain size proportion curves were created and analyzed. The same methodology was applied to measured sections from an IHS point bar outcrop (Durkin et al., in press) to evaluate trends of IHS deposits. Key outcomes of that study are used here as a foundation for potential modeling applications of heterolithic bayhead delta reservoirs.

Figure 3. Tibbet Canyon study area location map

A) Aerial photo of the southern Kaiparowits Plateau showing Tibbet Canyon field locations. Red dots show sections measured in this study (RPTC). Black box at the location of RPTC-2 outlines the bayhead delta area inset shown in Fig. 3B. The gray shaded inset is the outline of the Kaiparowits Plateau (Fig. 1) and the red box outlines the relative location of Fig. 3A.

B) Aerial photo showing the locations of measured sections TCIHS-1 to TCIHS-13 used for studying the continuous bayhead delta outcrop. This area also serves as the location for the terrestrial LiDAR model (Fig. 4). Rose diagram shows paleocurrent measurements from beds in the bayhead delta, indicating dominant northeast flow direction.

C) Schematic diagram showing the relative orientation of the outcrop measured section in Fig. 3B to the proposed depositional direction of the bayhead delta. The outcrop is exposed obliquely to the northeast depositional trend of the bayhead delta, so moving north along the outcrop permits analysis of the bayhead delta down dip, from topset to toset, and toward the delta depositional axis.



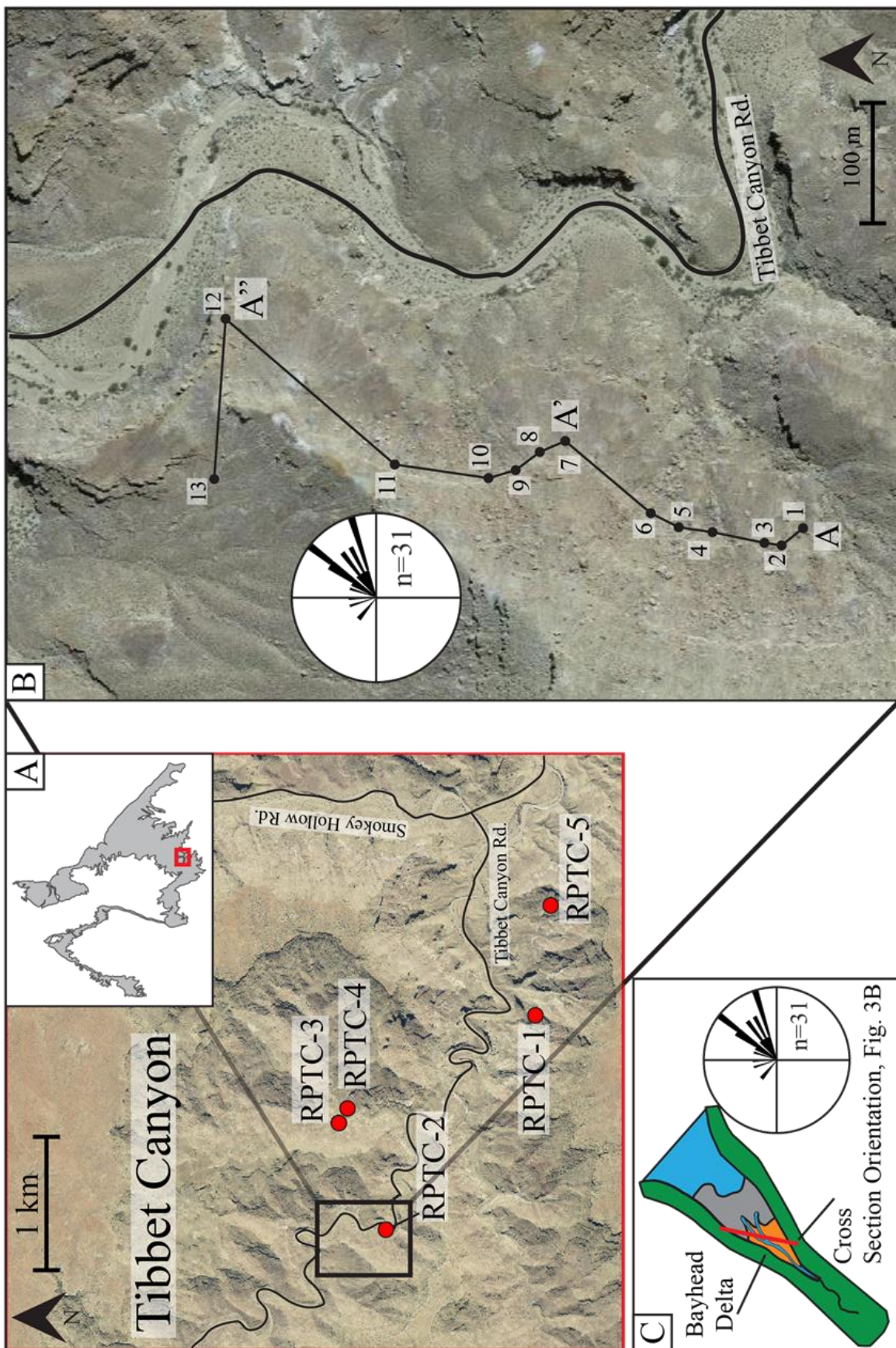
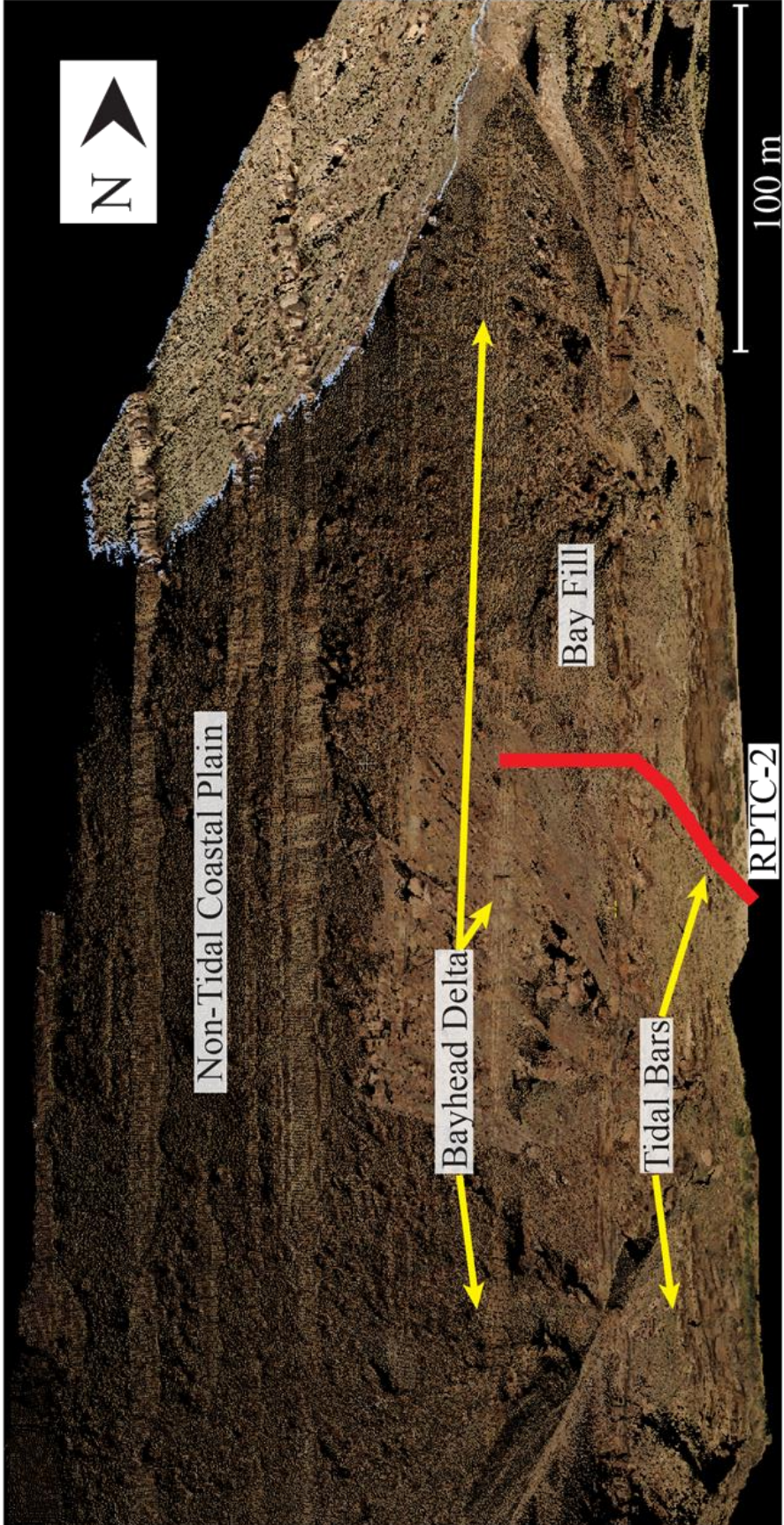




Figure 4. LiDAR outcrop interpretation of Tibbet Canyon measured section RPTC-2

Interpreted outcrop LiDAR model at RPTC-2. The base of the outcrop, at road level, shows heterolithic tidal bars of LA 1.1. Bay fill of LA 1.2 stratigraphically overlies the tidal bars. Bayhead delta deposits of LA 1.3 appear about 1/3 of the way up the outcrop, eroding into fine-grained deposits of the bay fill. Coastal plain of FA-3 comprises the remainder of the outcrop. Channel belts are visible throughout FA-3 and show increasing vertical and lateral amalgamation stratigraphically higher in the section, consistent with observations of upper John Henry Member fluvial channel trends in the southern Kaiparowits Plateau.



## RESULTS

### **Paralic Environment Facies Analysis**

Eight lithofacies assemblages (LAs) are identified based on lithology, primary sedimentary structures, bedding geometries, paleocurrent indicator measurements, trace and body fossils, and vertical and lateral relationships with other facies. Table 1 displays the detailed descriptions of each lithofacies assemblage. Figure 5 summarizes the hierarchical scheme applied in this study, showing the scales of observation and the associated level of interpretation. Lithofacies assemblages are essentially architectural elements (*sensu* Miall (1985a) and comprise a group of facies that commonly occur together, with recognizable spatial and geometric relationships. Because the main focus of this study is on meso-scale facies architecture and evolution of a bayhead delta, the bayhead delta lithofacies assemblage is further divided into its constituent components, which are described in detail following the hierarchical scheme of Nardin et al. (2013) (Fig. 6). This approach focuses on stratal stacking patterns and discontinuities. Stratal units include, in order of increasing scale, beds, bedsets, stories, progradational packages, and delta. Beds and bed sets are defined as time-stratigraphic units (Cambell, 1967; Nardin et al., 2013). However, in this study, the lateral accretion sets and bars of Nardin et al. (2013) become progradational packages and deltas to better reflect delta terminology. Lithofacies assemblages are grouped into three facies associations (FAs) according to their dominant depositional processes, ranging from tidal- to fluvial-dominated: estuary fill (FA-1), tide-

influenced coastal plain (FA-2), and non-tide influenced coastal plain (FA-3). Listed below, in stratigraphic order of occurrence, is a detailed description of facies associations and their interpreted depositional environments.

### *Facies Association 1*

Description. Facies association 1 (FA-1) (Fig. 7) occurs as part of the lower John Henry Member, directly overlying the Calico Bed, and has an average thickness of 37 m (ranging from 19-63 m). Lithofacies assemblages (LAs) of FA-1 include sigmoidal, channelized, bidirectional sandstones (LA 1.1) (Fig. 7A); interbedded mudstone, siltstone, sandstone, carbonaceous shale, and coal (LA 1.2) (Fig. 7B), and coarsening-upward inclined heterolithic strata (LA 1.3) (Figs. 8 and 9).

Deposits of LA 1.1 occur at the base of the John Henry Member, locally scouring down into the underlying Calico Bed, and consist of heterolithic sandstone and mudstone. Sandstone units are very fine- to fine-grained, have concave-upward erosive bases and display trough-cross stratification, planar-cross laminations, and ripple laminations. Trough-cross beds range from 20-60 cm thick and typically transition into ripple laminations. Rippled beds dominate LA 1.1 and range from 10 cm to 2 m thick. Mud or carbonaceous material often drapes ripples. Double mud drapes and flaser bedding are also common. Siltstone, mudstone, and carbonaceous shale interbeds are 5-10 cm thick. Trace fossils include *Lockeia* and *Planolites*. Beds of LA 1.1 display sigmoidal bedding and persistent mudstone drapes. Beds amalgamate to form lenticular bar complexes up to ~8 m thick that extend more than 100 m laterally. LA 1.1 reaches a maximum thickness of ~17 m (Fig. 7A). Paleocurrent indicators are scattered with dominant east-southeast

directed flow (Table 1).

Heterolithic deposits of LA 1.2 interfinger with LA 1.1 and are stratigraphically below LA 1.3. At its thickest, LA 1.2 is 40 m thick. Deposits of LA 1.2 consist of horizontal, tabular beds of mudstone, siltstone, carbonaceous shale, fine-grained sandstone, and sulfur-rich coal. Tabular sandstone beds range from 10-70 cm and contain ripple laminations (some climbing ripples), horizontal laminations, planar-cross laminations, convolute bedding, wood fragments, and mud drapes. Fine-grained sediment (siltstone and mudstone) dominates LA 1.2 and displays abundant trace fossils (e.g., *Thalassinoides*, *Planolites*, *Lockeia*, and bivalves). Isolated sandstone bodies up to 7 m thick are also present and are composed of fining-upward fine- to medium-grained sandstone beds with clay rip ups, current ripple laminations, planar-cross laminations, trough-cross stratification, and lateral accretion surfaces. Paleocurrent indicators from trough-cross beds show dominant flow toward the east and southeast, with lateral accretion toward the southwest and east (Table 1).

LA 1.3 is composed of very fine- to medium-grained sandstone beds with interbedded mudstone and siltstone that coarsen and thicken upward, creating a ~8.5 m thick complex. LA 1.3 deposits are stratigraphically above LA 1.2 and below FA-3. Mudstone and siltstone drapes are persistent and are organic-rich, containing leaf and plant fragments. Siltstone and sandstone beds with abundant leaf fossils and woody material also cap the coarsening-upward sequence. Sandstone beds dominantly contain ripple laminations, with flaser to wavy bedding, double mud drapes, and climbing ripples common. LA 1.3 trace fossils include *Thalassinoides*, *Teredolites*, *Planolites*, and *Lockeia*, as well as locally abundant wood fragments and leaf impressions (Fig. 7).

Inclined heterolithic strata are tabular to lenticular and inclined between 5° and 12°.

Tabular sandstones range 2-70 cm thick. Erosive channel sandstones up to ~2 m deep that have fine- to medium-grained trough-cross and planar-cross stratification incise into IHS beds. Paleocurrent indicators from ripples and trough-cross beds are dominantly unidirectional flowing to the north-northeast with accretion surfaces dominantly to the north-northwest (Table 1).

Interpretation: Estuary fill. FA-1 includes deposits of basal estuarine tidal bars (LA 1.1), central estuary bay fill (LA 1.2), and prograding bayhead delta (LA 1.3), marking the transition from a mixed-energy estuary to coastal plain. Convex-upward geometry, bimodal paleocurrent indicators, sigmoidal bedding, lateral accretion surfaces, and persistent mudstone drapes of LA 1.1 are indicative of deposition in tidal bars. Tidal bars are most commonly deposited as elongate bars in the outer estuary zone of tide-dominated estuaries (Dalrymple and Choi, 2007; Dalrymple, 2006; Dalrymple et al., 2012) or as elongate to lobate bars associated with bayhead deltas in mixed-energy estuaries (Steel et al., 2012).

LA 1.2 represents central estuary bay fill based on the stratigraphic association with LA 1.1 and 1.3, the brackish/marine trace and body fossils, and the heterolithic nature of the deposits. Preliminary findings from biostratigraphic samples indicate tidal influence, suggesting that these fine-grained sediments were deposited in a low energy lagoonal or bay environment (David Pocknall, 2015 personal communication). Central bay fill is typically composed of organic-rich fine-grained sediment, and occurs in the area of net bedload convergence as a result of interacting fluvial and marine energies (Boyd et al., 2006). In wave-dominated and mixed-energy estuaries, the central estuary bay fill is

dominated by heterolithic mudstone, siltstone, and sandstone (Mack et al., 2003). The prodelta facies of both flood-tidal deltas and bayhead deltas is equivalent to the central basin fill. Prodelta central basin fill may display fine-grained, organic-rich muds that are typically heavily bioturbated (Biggs, 1967; Donaldson et al., 1970). Increased sulfur content observed in central basin coal beds represents brackish water influence (Banerjee et al., 1996). Coals of this assemblage formed in tidal flats and ponds as part of the central bay. Crevasse or interdistributary channels are present within LA 1.2 as fining-upward, fine- to medium-grained isolated channel bodies with unidirectional trough-cross stratification that probably formed during storm events (Coleman and Prior, 1982). Paleocurrents show dominant flow toward the east (basinward) and southeast, with lateral accretion toward the southwest and east. The lack of tidal signatures (e.g., mud drapes, marine trace fossils) and dominantly unimodal paleocurrents perpendicular to accretion direction indicate fluvial-dominated deposition, similar to crevasse splay facies of interdistributary bay sequences (Elliott, 1974).

LA 1.3 comprises bayhead delta deposits based on the upward coarsening, inclined-heterolithic nature, ubiquitous mud drapes, moderate thickness, and relationship to organic-rich mudstones of LA 1.2 below and FA-3 above (Dalrymple et al., 1992; Plink-Björklund, 2008; Aschoff, 2009). The presence of brackish trace and body fossils and the dominantly basinward-directed paleocurrent indicators suggest that the sediment was derived from a terrestrial source and was deposited by rivers within a tide-influenced environment (Joeckel and Korus, 2012).

The lower John Henry Member bayhead delta interval at Tibbet Canyon was used for statistical analysis and reservoir characterization and modeling, and thus is interpreted

in detail here. Specifically, the bayhead delta facies of LA 1.3 are further divided into three architectural element categories: proximal prodelta, delta front, and delta plain. Included below is a description and interpretation of each of these architectural elements, which together represent the bayhead delta lithofacies assemblage (LA 1.3).

The proximal prodelta is characterized by thinly interbedded tabular mudstone, siltstone, and very fine-grained sandstone units, reaching a total maximum thickness of 4 m in the study area. Ripple laminations (including climbing ripples) dominate sandstone beds, which range in thickness from 1-27 cm. Siltstone and mudstone are laminated to massive, often have abundant carbonaceous material, and range from 1-31 cm thick. The prodelta is the area of a delta where fine mud and silt are deposited through suspension settling or by hyperpycnal flows (Bhattacharya, 2003). The preservation of silty and sandy laminations is thought to indicate the influence of river processes (Bhattacharya, 2003). Thin sandstone beds and thicker siltstones may represent frontal splays and slurry deposits which are fed from channel and bars farther upstream (Ahmed et al., 2014). Brackish to tidal indicators include double mud drapes and trace fossils such as *Thalassinoides*, *Teredolites*, *Planolites*, and *Lockeia*.

Delta front deposits consist of very fine- to fine-grained sandstone beds ranging from 0.02-1.9 m thick. Sedimentary structures include trough cross-stratification, ripple-laminations, planar cross-laminations, horizontal laminations, soft sediment deformation, and clay rip ups. Ripples display some mud draping as well as wavy to flaser bedding. Siltstone and mudstone range from 0.01-0.52 m thick and are laminated to massive with common carbonaceous material. Very fine- to fine-grained sandstone beds represent terminal distributary channels that dominate the delta front succession in the bayhead



delta of this study. Terminal distributary channels are characterized by trough cross-stratification and mud rip ups as well as erosive bases and variable low-topography (Olariu and Bhattacharya, 2006). The delta front deposits of river-dominated systems often consist of a complex association of terminal distributary channels and mouth bars (Bhattacharya, 2006). The apparent lack of mouth bars in this bayhead delta outcrop may be a result of erosion caused by the terminal distributary channels prograding basinward. In low accommodation settings, where channel flow depths and water depth are on the same scale, channels can more easily cannibalize the underlying deposits (Holbrook, 1996; Bhattacharya, 2006).

The delta plain is characterized by the presence of distributary channels with erosive u-shaped bases and flat tops which are typically filled with fining-upward heterolithic beds of mudstone, siltstone, and sandstone after channel switching and lobe abandonment has occurred (Bhattacharya, 2006). Channel forms erode into the underlying strata and scour up to several meters (~3 m). Beds deposited within the abandoned channel are tabular, horizontal, and onlap discordantly with the scour surface and the underlying delta front deposits. Sandstone beds are very fine- to fine-grained and have beds ranging from 2-38 cm in thickness that display ripple- and planar-laminations. Some ripples are wavy and mud draped, suggesting that there was some tidal influence acting within the channel. Toward the top of the delta plain, there are leaf impressions and organic fragments. Grain-size trends indicate a fining-upward facies succession, consistent with typical channel-fill facies models. The morphology of the deposit, as well as its erosive nature and heterolithic, mud-dominated fill, mark it as abandoned channel fill within the delta plain (Fig. 8).

## *Facies Association 2*

Description. Facies Association 2 (FA-2) (Fig. 10) is typically found in the lower to middle John Henry Member in Tibbet Canyon, averages about 21 m thick, and includes fining-upward IHS (LA 2.1) (Fig. 10A), and channelized, fining-upward, bidirectional, cross-stratified sandstones (LA 2.2) (Fig. 10B). Beds of LA 2.1 are composed of rhythmically interbedded siltstone, mudstone, and sandstone units. Facies primarily consist of very fine- to medium-grained sandstone displaying ripple laminations, planar-cross laminations, and local trough-cross stratification as well as convolute bedding, clay rip ups, and flaser/wavy/lenticular bedding. Siltstone beds display some ripple laminations. Mudstone drapes are pervasive, extend to the base of channel sequences, and are commonly organic rich and carbonaceous. Trace fossils include *Teredolites*, *Planolites*, *Lockeia*, *Thalassinoides*, and *Psilonichnus*. Erosion surfaces within the IHS often dip more steeply than adjacent strata, creating complex internal facies relationships (Fig. 10). IHS dip with angles between 5° and 15° and are continuous over tens to hundreds of meters laterally. Individual sandstone beds range from ~5 cm to 1 m, appear tabular, and thin laterally over tens to hundreds of meters into surrounding mudstone. Mudstone and siltstone beds range from 2-50 cm thick. Internal erosion surfaces are common within the sandstone beds, causing tens of cm to 1-2 m of local scour into underlying mudstone layer.

Beds of LA 2.2 are stratigraphically associated with LA 2.1 and are composed of heterolithic sandstone, siltstone, and mudstone. Sandstone beds range from fine- to coarse-grained and typically fine upward. Mudstone or siltstone often caps fining-upward sequences. Facies include trough-cross stratification, planar-cross stratification, ripple

laminations, flaser laminations, clay rip up clasts, convolute bedding, and wood fragments. Sandstone bodies are tabular or lenticular and display concave, erosive bases with lateral accretion sets and planar tops. Paleocurrent measurements from trough-cross beds in LA 2.2 show bidirectionality with dominant flow to the northeast and subordinate flow to the southwest (Table 1).

Interpretation: Tide-influenced coastal plain. Fining-upward IHS intervals represent deposits of laterally accreting point bars within tide-influenced rivers (LA 2.1). Studies throughout the Kaiparowits Plateau have identified tide-influenced fluvial IHS point bar deposits within fluvial-tidal portions of the John Henry Member (Shanley et al., 1992; Gallin et al., 2010; Gooley, 2010; Pettinga, 2013; Chentnik et al., in press). Laterally adjacent to IHS deposits of LA 2.1 are channelized, fining-upward trough-cross stratified sandstones with bidirectional paleocurrent indicators (LA 2.2), which have dominant basinward-directed (northeast to east) paleocurrents and subordinate flood-tidal oriented flow (southwest to west). Channels of LA 2.2 are dominantly fluvial in nature, with some tidal influence generating bidirectional paleocurrents.

The rhythmic interbedding of sandstone and finer-grained mudstone of LA 2.1 reflects fluctuating current energies and variations in fluvial and tidal influence (Thomas et al., 1987; Shanley et al., 1992). Mudstone beds likely represent deposition during slack water periods between diurnal tidal cycles (Bridges and Leeder, 1976), or seasonal fluctuations in discharge with changes in spring and neap tides (Dalrymple and Choi, 2007; de Mowbray, 1983). Such deposits have been identified in fluvial environments with no marine influence (Jackson, 1981; Page et al., 2003). However, due to the presence of marine/brackish trace fossils (*Lockeia*, *Thalassinoides*, and *Teredolites*) and

double mud drapes, LA 2.1 is interpreted as tide-influenced channels and interdistributary deposits.

### *Facies Association 3*

Description. Facies association 3 (FA-3) (Fig. 11) dominates the upper John Henry Member of Tibbet Canyon. Measured section RPTC-2 is the only section that measured to the Drip Tank Member (thus capturing the full thickness of the John Henry Member). Although not central to the evolution of paralic strata, FA-3 is included here as it relates to regional correlations. The thickness of FA-3 was 175 m from the top of FA-2 to the base of the Drip Tank Member. Where FA-3 is present in the lower John Henry Member it has an average thickness of 22 m (ranging from 12-37 m).

FA-3 contains lithofacies assemblages of channelized, upward-fining, cross-stratified sandstones (LA 3.1), interbedded mudstone, siltstone, and sandstone (LA 3.2), and coal and carbonaceous shale (LA 3.3). LA 3.1 sandstone beds are capped by mudstone or siltstone, ranging from fine- to coarse-grained, and typically fine upward. Facies include trough-cross stratification, planar-cross stratification, ripple laminations, flaser laminations, clay rip up clasts, convolute bedding, and wood fragments. Coarse-grained pebble gravel lags, as well as coarse-grained trough cross beds with pebble lags along trough foresets, are also present. Channel sequences are commonly capped by convex, erosive-based, U-shaped features with heterolithic fill consisting of horizontal, tabular beds of mudstone and interbedded very fine-grained sandstone. Sandstone bodies of LA 3.1 are tabular or lenticular and have concave, erosive bases with lateral accretion sets and planar tops. Sandstone beds are up to ~10 cm thick, display ripple laminations,

and are laterally discontinuous, forming ribbon-like beds. Upward-fining, cross-stratified sandstones of LA 3.1 occur as isolated, single-story channels. Channels range from 1-6 m thick and are laterally continuous for hundreds of meters. Paleocurrents are dominantly eastward but show a wide range from northeast- to southeast-directed flow (Table 1).

Horizontal, tabular beds of interbedded mudstone and siltstone dominate LA 3.2 with a few isolated sandstones beds. Mudstone and siltstone beds are predominantly massive or laminated. Some beds display mottling or nodular concretions. Organic-rich mud and carbonaceous shale are also common in this assemblage, and in some cases, these facies grade vertically into coal. Very fine- to fine-grained sandstones range from 2 cm to 1 m thick with massive bedding, ripple laminations, and horizontal laminations. Root traces commonly penetrate the tops of sandstone beds, and plant fragments are present throughout this association. *Planolites* is present but uncommon, and a gastropod shell was identified in float of this association.

LA 3.3 is composed of discontinuous, horizontal, tabular, organic-rich deposits of coal and carbonaceous shale. Deposits are typically sulfur-rich and contain abundant plant material and leaf fragments. Individual coals range from a <5 cm up to 50 cm thick in places, but deposits of LA 3.3, including both coal and carbonaceous shale, may be a few meters thick.

Interpretation: Coastal plain. FA-3 preserves fluvial channel belts (LA 3.1) and associated coastal plain deposits (LA 3.2, 3.3). Regional correlations suggest that deposition of the John Henry Member occurred as part of a fluvial megafan or distributive fluvial system (Szwarc et al., in press), as discussed below. Lack of tidal influence distinguishes FA-3 from FA-2. Channel bases form sharp, erosive contacts with

underlying floodplain facies assemblages or other channel forms. Channels may amalgamate laterally and/or vertically to form single-story and multistory channel belts, respectively. Internal scour surfaces, lateral barform accretion surfaces, and unidirectional trough-cross stratified paleocurrent indicators are indicative of fluvial channels (Miall, 1985a). Floodplain (LA 3.2) and coal mire (LA 3.3) assemblages interfinger laterally and cap channel form deposits.

LA 3.2 represents interdistributary floodplain deposits due to its relationship with LA 3.1 and LA 3.3, lack of marine indicators, and presence of root traces and abundant plant material. Deposits consist of tabular beds of mudstone, siltstone, and sandstone. Architectural elements that comprise this assemblage include the fine-grained sandstone beds, which can be levee or crevasse-splay deposits (depending on their relationship to channel deposits), floodplain fines, and/or soil horizons (Miall, 2006; Bridge, 2003). Mottling and nodular concretions present in the siltstone and mudstone are indicative of early stages of diagenesis and potential soil development (Driese et al., 2010; Suarez et al., 2010). Heterolithic overbank deposits of mudstone, siltstone, and sandstone of LA 3.2 fill local sequences of abandoned channel deposits, which display the concave, erosive bases typical of fluvial channels. Sediment filling the abandoned channel is the result of suspended and bedload deposition during flood events, and subsequent ponding in the topographic low created by the channel (Hooke, 2004; Kraus and Davies-Vollum, 2004). Coal and carbonaceous shale of LA 3.3 are coal mires, which can develop as part of floodplain, coastal plain, delta plain, and back-barrier environments (Thornton, 1979; Thomas, 2012; Horne et al., 1978). Coals of this assemblage represent swampy interdistributary areas adjacent to fluvial channels.

### **Analysis of Spatial Data from the Bayhead Delta Reservoir Analog**

Bayhead delta deposits from FA-1 contribute data for statistical analysis and serve as outcrop analogs to subsurface reservoirs. Five major surfaces and four progradational packages (P1, P2, P3, and P4) define the bayhead delta interval of interest. Eleven stories exist within the four progradational packages shown in Fig. 9 and 12. The base of the bayhead delta hangs on the top of a continuous coal surface that extends throughout the length of the outcrop exposure. The top bayhead surface is a gradational boundary marking the transition from delta processes to coastal plain. Some measured sections were unable to capture the top bayhead surface due to poor outcrop exposure. Where the outcrop is covered, LiDAR and photomosaics allowed for extrapolation of the top surface.

A model was created using the stratigraphic hierarchy and measured sections to help visualize and quantify the architectural and facies relationships of the bayhead delta. The model used a 5 cm grid layer discretization, and grain size was averaged for each measured section to match the coarser 5 cm sampling of the grid. The model has 270 layers which track grain size variations within each story. Internal layering and packages serve as the stratigraphic framework to perform statistical characterization. These include grain size, amalgamation ratio (AR), net-to-gross (NTG), and average bedding thicknesses for each individual package, as well as the bayhead delta as a whole. Analysis was performed along the packages from proximal to distal and then from package to package, in stratigraphic order, to elucidate the evolution of the system. Identifying trends between individual stories is difficult, and therefore the bulk of the discussion of statistical analysis focuses on package relationships.

*Lateral Trends (Down-Dip) (Fig. 13)*

Figure 13 explores the spatial and temporal relationship of the outcrop package statistics. Each x-axis shows the distance along the outcrop from the origin at measured section TCIHS-1. Because the outcrop is exposed obliquely to the northeast depositional trend of the bayhead delta, moving along the outcrop from the point of origin allows for analysis of the packages, down dip, from topset to toset, and toward the delta depositional axis (Fig. 3). Specific analysis of P4 is not included due to the general lack of bed measurements from sections through this package. The number of beds described in each measured section and used in the calculation of the following metrics can be found in Table 2.

Amalgamation ratio (AR). An amalgamation surface is defined as sandstone on sandstone contact between individual event beds (Romans et al., 2009; Fletcher et al., 2011). Amalgamation ratio (AR) is equal to the number of amalgamation surfaces in a channel element divided by the total number of sedimentation units minus one. Minimum AR calculated in a measured section is 0.0, where none of the beds have amalgamated surfaces. P1 has a weakly negative AR trend with poor correlation ( $R^2 = 0.26$ ). P2 and P3 both have positive overall AR trends along the extent of the outcrop and moderate correlation values (P2:  $R^2 = 0.5$ , P3:  $R^2 = 0.7$ ). However, P2 and P3 both show complexity from location to location in their AR. This likely reflects the complex nature of delta front distributary channel systems. P2 and P3 both have low AR topset values. AR rapidly increases along the outcrop toward the toset and the delta depositional axis, where all the beds are amalgamated. Siltstone and shale dominate P4, with some sandstone beds interbedded. However, P4 does not contain any amalgamated beds.

Average bed thickness. Average bed thickness is a measurement that takes into



account the thicknesses of all the beds in a given package. Displayed on the graph of Figure 13B is the average bed thickness for a package measured for each measured section. The minimum bed thickness measured in each section was 1 cm. Package 1-4 presents an increase in average bed thickness of all beds measured from the top to the base of the package and along the extent of the outcrop. P1 has a maximum bed thickness of 85 cm with an average bed thickness per measured section ranging from 6-35 cm. Bed thickness of P2 reaches 190 cm with an average bedding thickness from 7-97 cm. Average bedding thickness of P3 ranges from 10-118 cm and has a maximum bedding thickness of 190 cm, which is the thickest of the bayhead delta sandstone deposits. As the system progresses from stratigraphically older to younger, each package displays a higher average bedding thickness.

Net-to-gross (NTG). Net-to-gross (NTG) is defined as the thickness of sandstone divided by gross thickness of the interval of interest. P1, P2, and P3 display increasing NTG trends from topset to toeset along the outcrop (Fig. 13C). The abandoned channel of P4 formed as the last phase of delta occupation and represents the dominantly passive filling after sediments were already diverted away and the delta was abandoned. Prodelta deposits of P1 have a higher average NTG than the abandoned channel fill (avg. = 0.66), with NTG ranging from 0.47 to 0.85, but still lower than the delta front deposits (P2 and P3). The prodelta deposits represent initial delta deposition and are comparatively distal to the sediment input. Therefore, they are characteristically fine-grained. However, delta front deposits show similar maximum NTG, reaching a maximum of 1.00, but have large ranges. P2 ranges from 0.54 to 1.00 (avg. = 0.77) and P3 ranges from 0.14 to 1.00 (avg. = 0.57). Delta front deposits typically have higher NTG than the prodelta because they are

more proximal to sediment input and are deposited under higher energy conditions than the prodelta. NTG generally increase along the outcrop as the system progrades and moves toward the depositional axis.

### *Vertical Trends (Fig. 13)*

Grain size. Using the geometric model derived from the outcrop interpretation, grain size probability curves were computed for each story and layer within the model. The model allows for bed-parallel analysis, examining from the top of the layer to the base along the full length of the package in order to observe how grain sizes are distributed within each package. The result is a proportion of grains distributed along a single depositional bed (within the package from topset to toset) leading to an understanding of how the grain size proportions change for each depositional layer within a package. These relationships between the various packages and stories in the bayhead delta are discussed below.

Each of the prodelta stories (1.1-1.3) of package 1 (P1) coarsens upward, and there is an overall coarsening-upward of the entire package. The bottom portion of package 2 (P2), delta front, is similar to the prodelta (2.1 and 2.2) with consistent coarsening-upward stories, but becomes more variable toward the top (2.3 and 2.4) with a higher proportion of coarser grains in story 2.3 and multiple cycles of very-fine sandstone in package 2.4. P2 as a whole also shows a general coarsening-upward grain size proportion trend. Delta front package three (P3) shows a general fining-upward trend and is overall finer-grained than P2. The basal P3 stories (3.2 and 3.3) individually coarsen upward, but story 3.3 fines upward, and each story is finer-grained than the underlying story. Package four (P4), delta plain abandoned channel fill, has a fining-upward grain

size proportion curve, and is the finest- grained of all the packages. The overall grain size trend of the bayhead delta generally coarsens upward from the basal P1 prodelta to the top of P2 delta front and is slightly finer-grained in P3 delta front with abrupt fining occurring in the P4 abandoned channel.

Figure 5. Facies hierarchy

Organizational facies hierarchy employed in this study with increasing scales of observation and associated levels of interpretation. This scheme is modified after Miall (1985a) and Nardin et al. (2013).

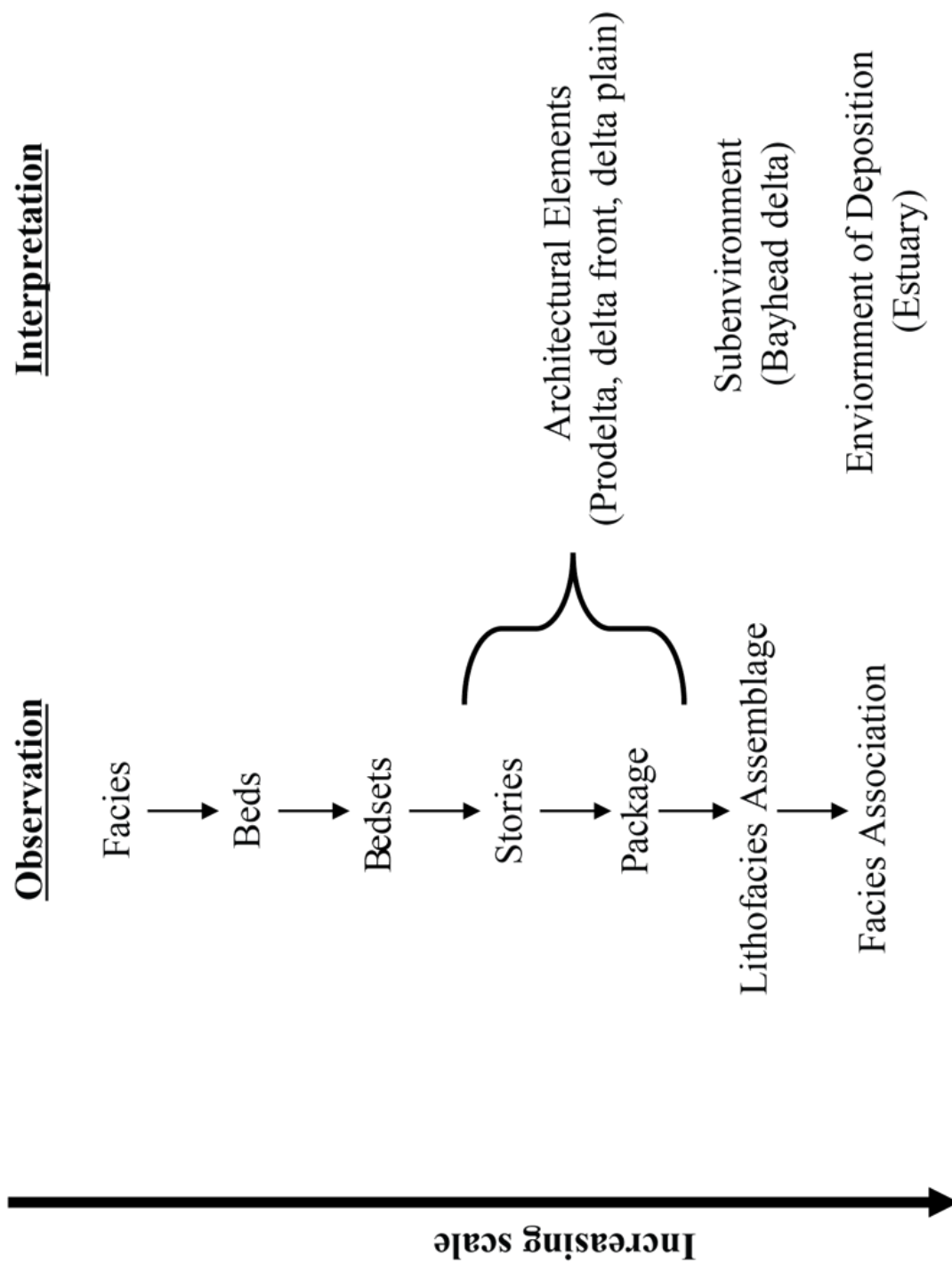


Figure 6. Bayhead delta bedding hierarchy

Bayhead delta bedding hierarchy scheme detailing arrangement of beds, bedsets, stories, progradational packages, and deltas. Application of the hierarchy is shown on the outcrop image to the right, following the measured section path of TCIHS-5 with the beds of this section illustrated on the left. Measured section reaches a height of 7 m.

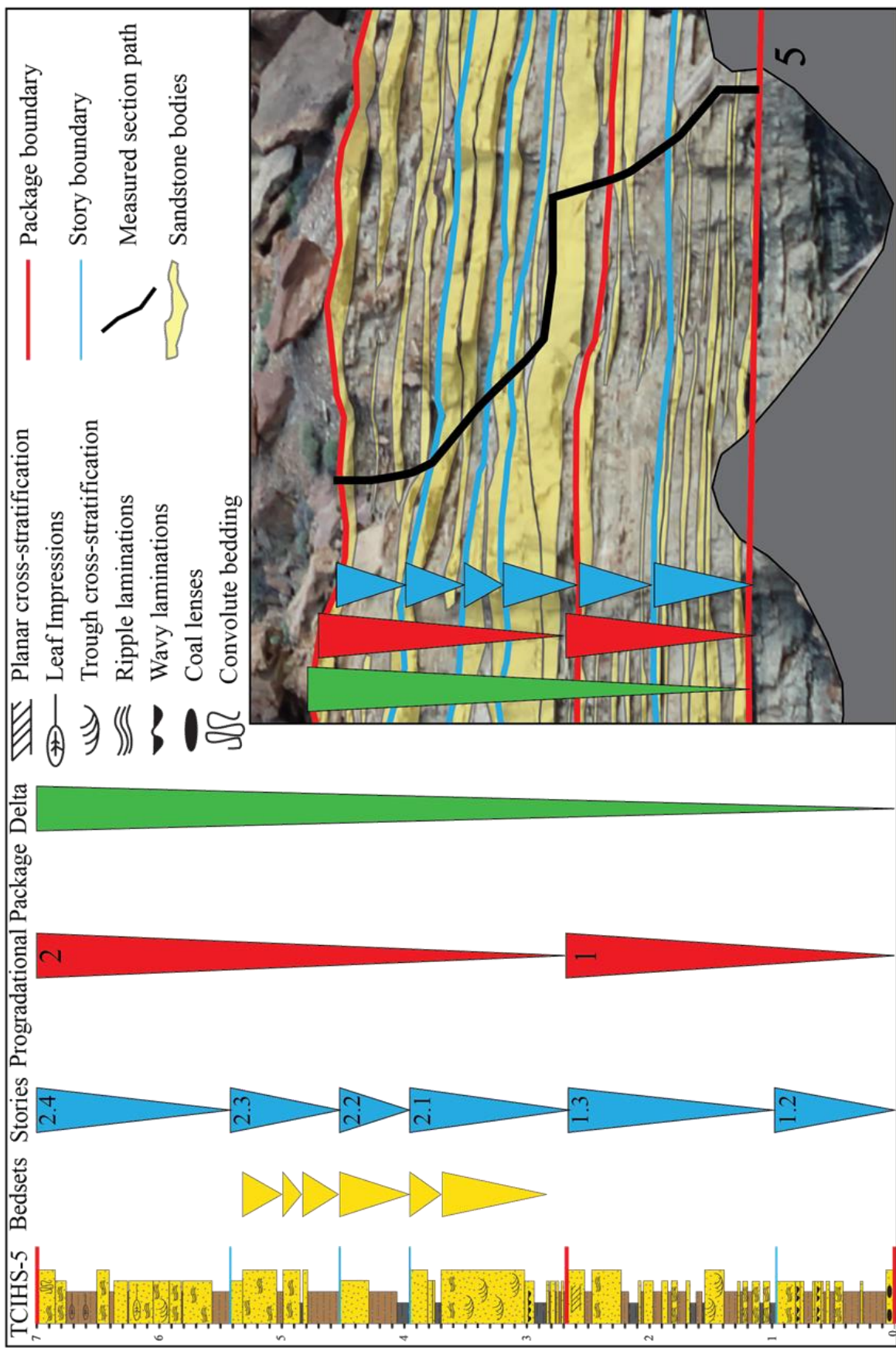


Table 1  
Lithofacies descriptions and environmental interpretations  
*Facies Association 1 - Estuary Fill*




Lithofacies Assemblage	Description and Architecture	Trace/Body Fossils	Interpretation
<ul style="list-style-type: none"> <li>• Sigmoidal, lenticular, sandstone beds separated by persistent mudstone interbeds</li> <li>• Concave-upward, erosive, very fine- to fine-grained sandstone with trough-cross stratification, planar-cross stratification, and ripple lamination</li> <li>• Trough-cross beds range from 20-60 cm thick and typically transitions into ripple laminated</li> <li>• Rippled beds dominate and range from 10 cm to 2 m thick</li> <li>• Ripples often draped with mudstone or carbonaceous material</li> <li>• Double mud drapes and flaser bedding common</li> <li>• Mudstone, siltstone, and carbonaceous shale interbeds are 5-10 cm thick</li> <li>• Scattered paleocurrents indicate tidal influence</li> <li>• Beds amalgamate to form lenticular bar complexes up to ~ 8 m thick</li> <li>• Maximum thickness of ~ 17 m</li> </ul> <p><b>1.1 - Sigmoidal, channelized bidirectional sandstones</b></p>	<p><i>Lockeia</i> and <i>Planolites</i>.</p>  <p>n=41</p>	<p><b>Tidal bars</b></p>	
<ul style="list-style-type: none"> <li>• Horizontal, tabular beds of mudstone, siltstone, carbonaceous shale, fine-grained sandstone, and coal</li> <li>• Tabular sandstone beds range from 10-70 cm</li> <li>• Sandstone beds have ripple laminations (some climbing), horizontal and planar-cross stratification</li> <li>• Abundant marine/brackish fossils</li> <li>• Isolated fining-upward fine- to medium-grained sandstone channel bodies, up to 7 m thick</li> <li>• Channel sandstones have clay rips ups, ripples, planar-cross stratification, trough-cross stratification, Paleocurrent indicators from trough-cross beds show E-SE flow and lateral accretion SW and E</li> <li>• Up to ~ 40 m thick</li> <li>• Coarsening-/thickening-upward inclined, tabular to lenticular, heterolithic beds</li> <li>• Very fine- to medium-grained sandstone with interbedded mudstone and siltstone</li> <li>• Organic rich mudstone and siltstone drapes persistent throughout</li> </ul> <p><b>1.2 - Interbedded mudstone, siltstone, sandstone, carbonaceous shale, and coal</b></p>	<p><i>Thalassinoides</i>, <i>Planolites</i>, and <i>Lockeia</i> traces present. Wood fragments are frequent and bivalves are rare.</p>  <p>n=119</p>	<p><b>Central bay fill and crevasse channels</b></p>	
<ul style="list-style-type: none"> <li>• Sequence capped by siltstone and sandstone beds with abundant leaf fossils and woody material</li> <li>• Tabular sandstones range 2-70 cm thick</li> <li>• Ripple dominated, with flaser to wavy bedding, double mud drapes, and climbing ripples common</li> <li>• IHS beds inclined 5° - 12° and are cut laterally by erosive channel sandstone up to ~ 2 m deep</li> <li>• Fine- to medium-grained trough-cross and planar-cross stratified sandstone beds</li> <li>• N-NE unidirectional ripple laminated and trough-cross stratified sandstone paleocurrent indicators and accretion surfaces N-NW</li> </ul> <p><b>1.3 - Coarsening-upward inclined heterolithic strata</b></p>	<p><i>Thalassinoides</i>, <i>Teredolites</i>, <i>Planolites</i>, and <i>Lockeia</i>. Wood fragments common and leaf fossils locally abundant within beds capping the sequence.</p>  <p>n=31</p>	<p><b>Bayhead delta</b></p>	



Table 1 (continued)  
Lithofacies descriptions and environmental interpretations  
*Facies Association 2 – Tide-influenced Coastal Plain*

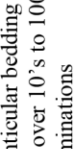
Lithofacies Assemblage	Description and Architecture	Trace/Body Fossils	Environment
<ul style="list-style-type: none"> <li>Rhythmically interbedded beds of mudstone, siltstone, and sandstone inclined 5°-15°</li> <li>IHS continuous over 10's to 100's of m laterally</li> <li>Very fine- to medium-grained ripple laminated, planar-cross stratified, trough-cross stratified sandstone dominate</li> </ul>		<p><i>Teredolites</i>, <i>Planolites</i>, <i>Lockeia</i>, <i>Thalassinoides</i>, and <i>Pylonichmus</i>.</p>	<p>Tidally influenced point bar</p>
<p><b>2.1 - Fining-upward inclined heterolithic strata</b></p> <ul style="list-style-type: none"> <li>Convolute bedding, clay rip ups, and flaser, wavy, and lenticular bedding also present</li> <li>Tabular sandstone beds ~ 5 cm to 1 m thick thin laterally over 10's to 100's of m into mudstone</li> <li>Siltstone beds laminated and sometimes display ripple laminations</li> <li>Mudstone drapes pervasive and extend to the base of channel sequences</li> <li>Mudstone commonly organic-rich and carbonaceous</li> <li>Mudstone and siltstone beds range from 2-50 cm thick</li> <li>Internal erosion surfaces common within the sandstone, causing 10's of cm to 1-2 m of local scour</li> </ul>			 <p>n=65</p>
<p><b>2.2 -Channelized, upward-fining, bidirectional cross-stratified sandstones</b></p> <ul style="list-style-type: none"> <li>Tabular/lenticular sandstone with erosive bases, lateral accretion sets and planar tops</li> <li>Fine- to coarse-grained, typically fining upward sandstone capped by mudstone or siltstone</li> <li>Trough-cross stratified, planar-cross stratified, ripple laminated sandstone with flaser laminations, clay rips up clasts, convolute bedding, and wood fragments</li> <li>Bidirectional paleoflow dominantly NE and subordinate flow SW</li> </ul>		<p><i>Lockeia</i> and <i>Planolites</i>. Plant material and leaf fragments.</p>	<p>Tidally influenced fluvial channel</p>

Table 1 (continued)  
Lithofacies descriptions and environmental interpretations  
*Facies Association 3 – Non Tide-influenced Coastal Plain*


Lithofacies Assemblage	Description and Architecture	Trace/Body Fossils	Environment
<ul style="list-style-type: none"> <li>• Tabular/lenticular sandstone with erosive bases, lateral accretion sets, and planar tops</li> <li>• Fine- to coarse-grained sandstone typically fining-upward and capped by mudstone or siltstone</li> <li>• Sandstone is trough-cross stratified, planar-cross stratified, ripple laminated with flaser laminations, clay rip up clasts, convolute bedding, and wood fragments</li> <li>• Coarse-grained pebble gravel lags and trough-cross stratified sandstone with pebble foresets present</li> <li>• Channel sequences capped by U-shaped, fine-grained heterolithic fill</li> <li>• Channels range from 1-6 m thick and are laterally continuous for hundreds of meters</li> </ul> <p><b>3.1 - Channelized, upward-fining, cross-stratified sandstones</b></p>		<p><i>Planolites</i></p>	<p><b>Fluvial channels</b></p>  <p>n=119</p>
<ul style="list-style-type: none"> <li>• Horizontal, tabular beds of interbedded mudstone and siltstone with occasional sandstone</li> <li>• Mudstone and siltstone predominantly massive or laminated with some mottling or nodular concretions</li> <li>• Organic rich mud and carbonaceous shale common and sometimes grades vertically into coal</li> <li>• Very fine- to fine-grained sandstone beds range from 2 cm to 1 m thick with massive bedding, ripple laminations, and horizontal stratification</li> </ul> <p><b>3.2 - Horizontal, tabular beds of interbedded mudstone, siltstone, and sandstone</b></p>		<p><i>Planolites</i> present, but uncommon. Gastropod shell identified in float.</p>	<p><b>Floodplain</b></p>
<ul style="list-style-type: none"> <li>• Root traces commonly penetrate tops of sandstone beds and plant fragments are common</li> <li>• Discontinuous, horizontal, tabular, organic-rich deposits of coal and carbonaceous shale</li> <li>• Deposits are typically sulfur-rich and contain abundant plant material and leaf fragments</li> <li>• Individual coals range from a &lt;5 cm up to 50 cm thick</li> <li>• Coal and carbonaceous shale sequences may be a few m's thick</li> </ul> <p><b>3.3 - Coal and carbonaceous shale</b></p>		<p>Plant material and leaf fragments.</p>	<p><b>Coal mire</b></p>

Figure 7. Estuary fill facies

Photomosaic of estuary fill facies (FA-1). A) Heterolithic tidal bars found in LA 1.1 at the base of RPTC-2, directly overlying the Calico Bed. B) Heterolithic bay fill and crevasse channel of LA 1.2. C) Flaser bedding and ripples laminations. Sub-horizontal *Planolites* trace featured prominently in the center of the image. D) Double mud drapes. E) Bivalve fossils preserved in siltstone of LA 1.2. F) Leaf impression in mudstone. G) Organic wood fragments and coal lenses. H) Abundant horizontal *Planolites* traces preserved as positive relief on the base of very fine-grained sandstone beds. I) Almond-shaped *Lockeia* trace fossils on the base of a fine-grained sandstone bed. J) Large *Teredolites* exposed in the remnants of a large log.

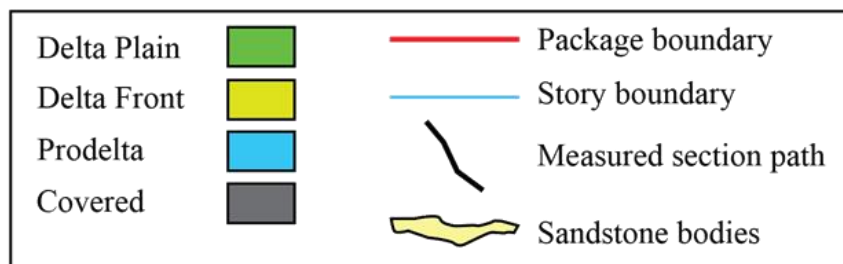
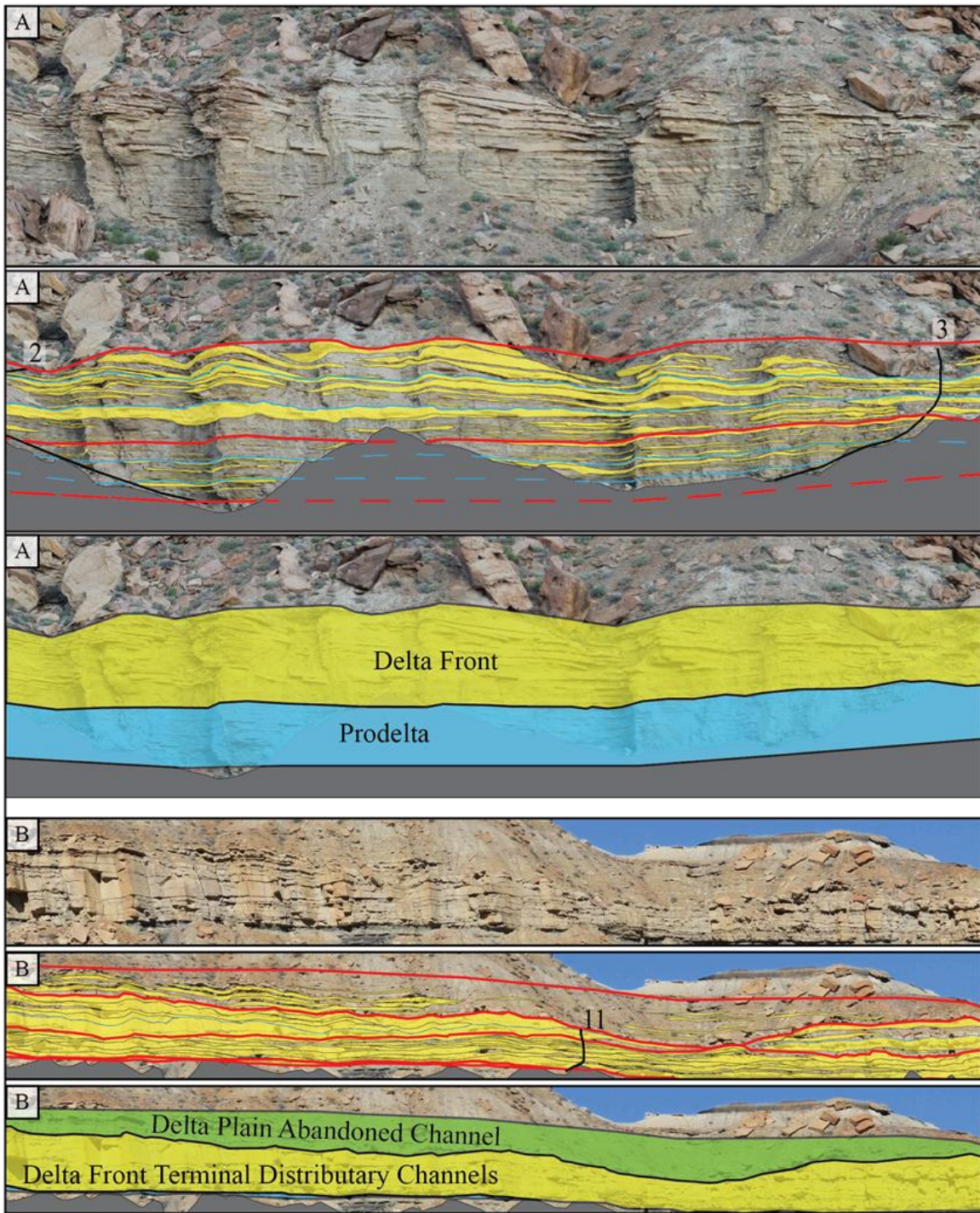




Figure 8. Bayhead delta facies

Outcrop diagram of inset views from Fig. 7. Each image shows an uninterpreted (top) outcrop image, a sand distribution overlay (middle), and a depositional subenvironment interpretation (bottom). 8a) Southern, up-dip exposure of bayhead delta displaying typical coarsening upward prodelta to delta front vertical profile.





#### Figure 9. Bayhead delta outcrop interpretation

Outcrop diagram of Tibbet Canyon bayhead delta used for stratigraphic analysis of inclined heterolithic strata. A to A' shows the southern outcrop face exposure and A' to A'' shows the northern extent of the exposure, resulting in ~ 600 m of continuous outcrop in this image. Each panel consists of an uninterpreted outcrop image (top), a sand distribution overlay (middle), and a hierarchical story interpretation (bottom). Black lines show the measured section paths of TCIHS 1-12, and measurements from these sections use sedimentology and spatial inputs for the bayhead delta model. Red boxes correspond to perspectives of the outcrop examining detailed bayhead delta facies in Fig. 8a and 8b respectively.



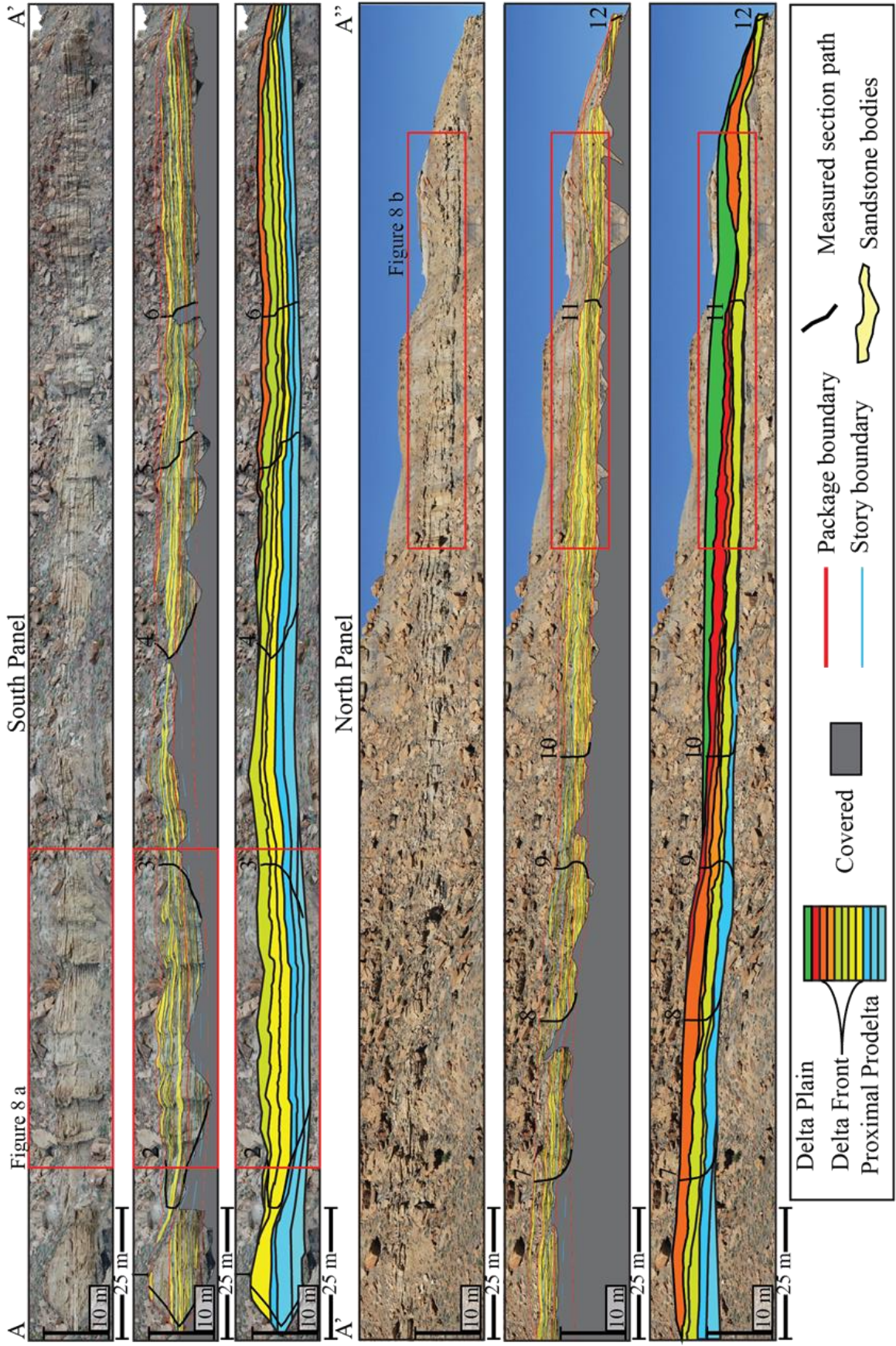




Figure 10. Tide-influenced coastal plain facies

Photomosaic of tide-influenced coastal plain facies (FA-2). A) Tide-influenced fluvial IHS point bar. B) Bidirectional herringbone cross-stratification indicative of alternating flow directions. C) Flaser to wavy bedding. Interlaminated sandstone and mudstone with mud-draped ripples. D) *Lockeia* traces preserved on the base of a fine-grained sandstone bed. E, F, G) increasingly detailed perspectives of tide-influenced fluvial point bar highlighting the varying scales of heterogeneity and local scour possible for these deposits. H) Trough cross-stratified medium-grained sandstone. I) *Psilonichnus* trace fossil preserved in fine-grained sandstone bed of IHS point bar. J) *Teredolites* trace exposed in fine-grained sandstone bed of IHS point bar.

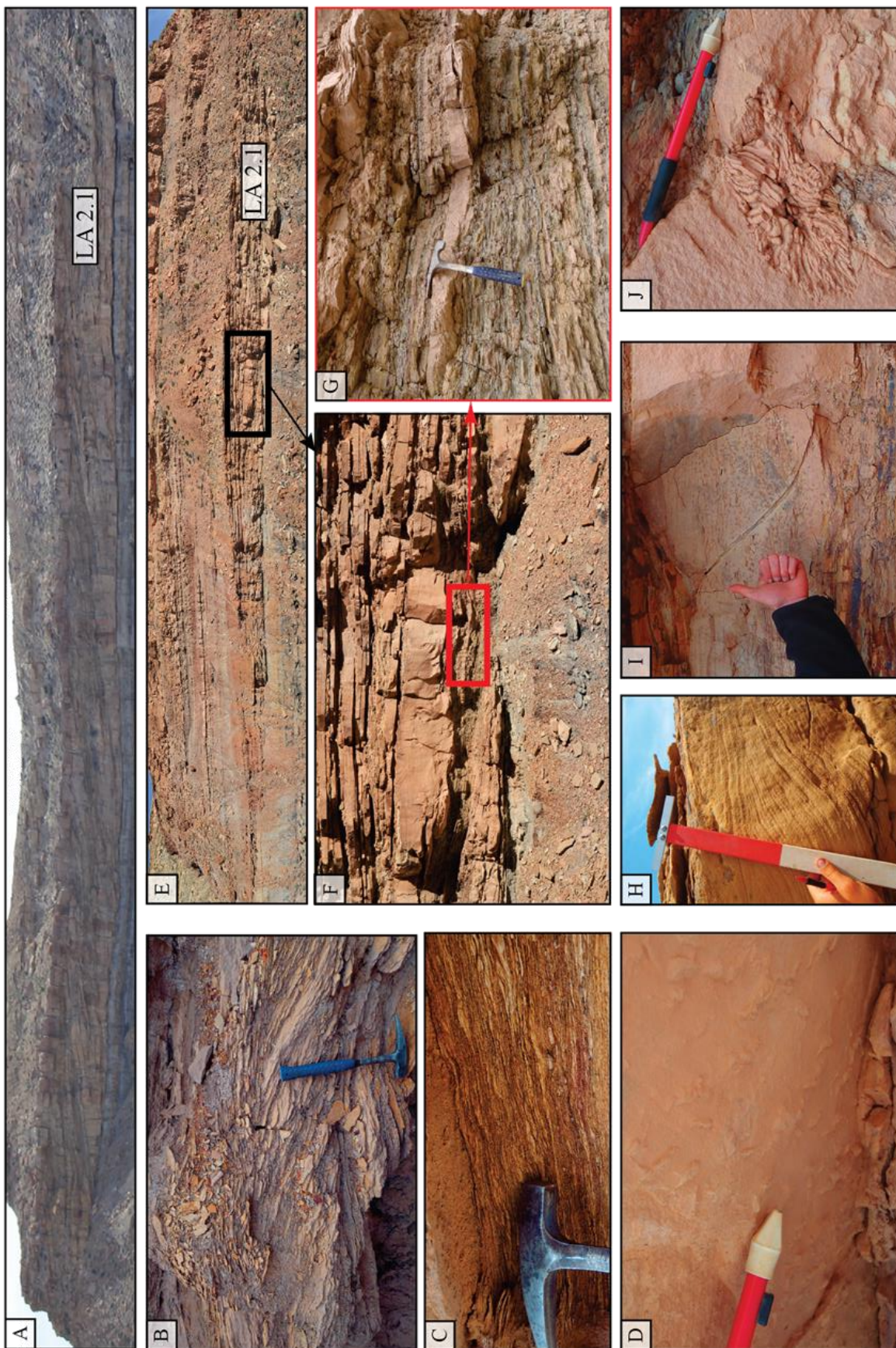


Figure 11. Coastal plain facies

Photomosaic of coastal plain facies (FA-3). A) Fluvial channel belt eroding into floodplain fines. B) Fluvial channel belt displaying internal scour. Channel belt is eroding into underlying coal mire facies. C) Coarse-grained trough cross-stratified fluvial channels with some gravel concentrated along cross-strata foresets. D) Trough-cross stratified, fine-grained sandstone. E) Convolute bedding in fine-grained sandstone displaying soft sediment deformation flame structures. F) Carbonaceous shale. G) Ripple-laminated, fine-grained sandstone. Coarse-grained sandstone to granule bed. I) Dark gray, organic-rich siltstone.



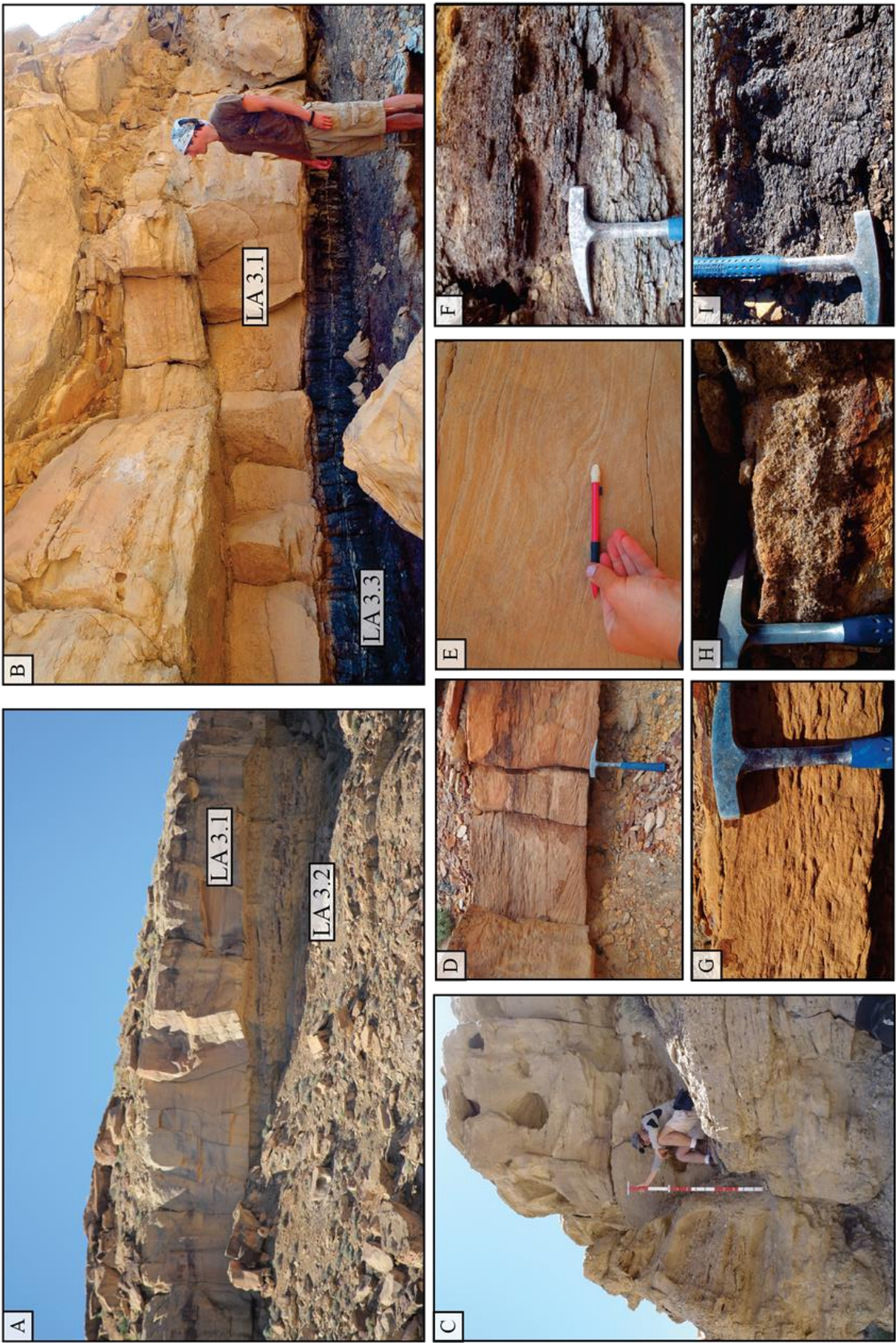


Figure 12. Bayhead delta measured section correlation

Measured section correlation of bayhead delta sections TCIHS 1-12. Proximal prodelta stories show progradational stacking with the top of each story downlapping onto the bay floor. Delta front appears to be more lenticular, with individual stories pinching out or eroding overlying stories (e.g., stories 2.2, 3.1, and 3.3). Abandoned channel fill erodes into the delta front up to ~3 m, removing delta front sandstones and replacing them with fine-grained sediments.



Table 2

		Number of Beds Per Measured Section for Spatial Data Analysis												
		<b>1</b>	<b>2</b>	<b>3</b>	<b>4</b>	<b>5</b>	<b>6</b>	<b>7</b>	<b>8</b>	<b>9</b>	<b>10</b>	<b>11</b>	<b>12</b>	<b>13</b>
Package	<b>3</b>	0	0	0	0	0	6	6	32	46	32	3	3	2
	<b>2</b>	13	45	32	30	38	35	25	21	12	13	13	3	3
	<b>1</b>	52	35	32	54	42	38	32	10	5	8	0	0	0

Figure 13. Lateral outcrop statistical trends

Graphs of outcrop statistical trends calculated for each measured section from the point of origin of the bayhead delta outcrop exposure on the x-axis. Statistics are broken out by package, with package one (P1) proximal prodelta and delta front of package two and three (P2 and P3). Featured are lateral trends in amalgamation ratio (AR, top), average bed thickness (middle), and net to gross ratio (NTG, bottom).



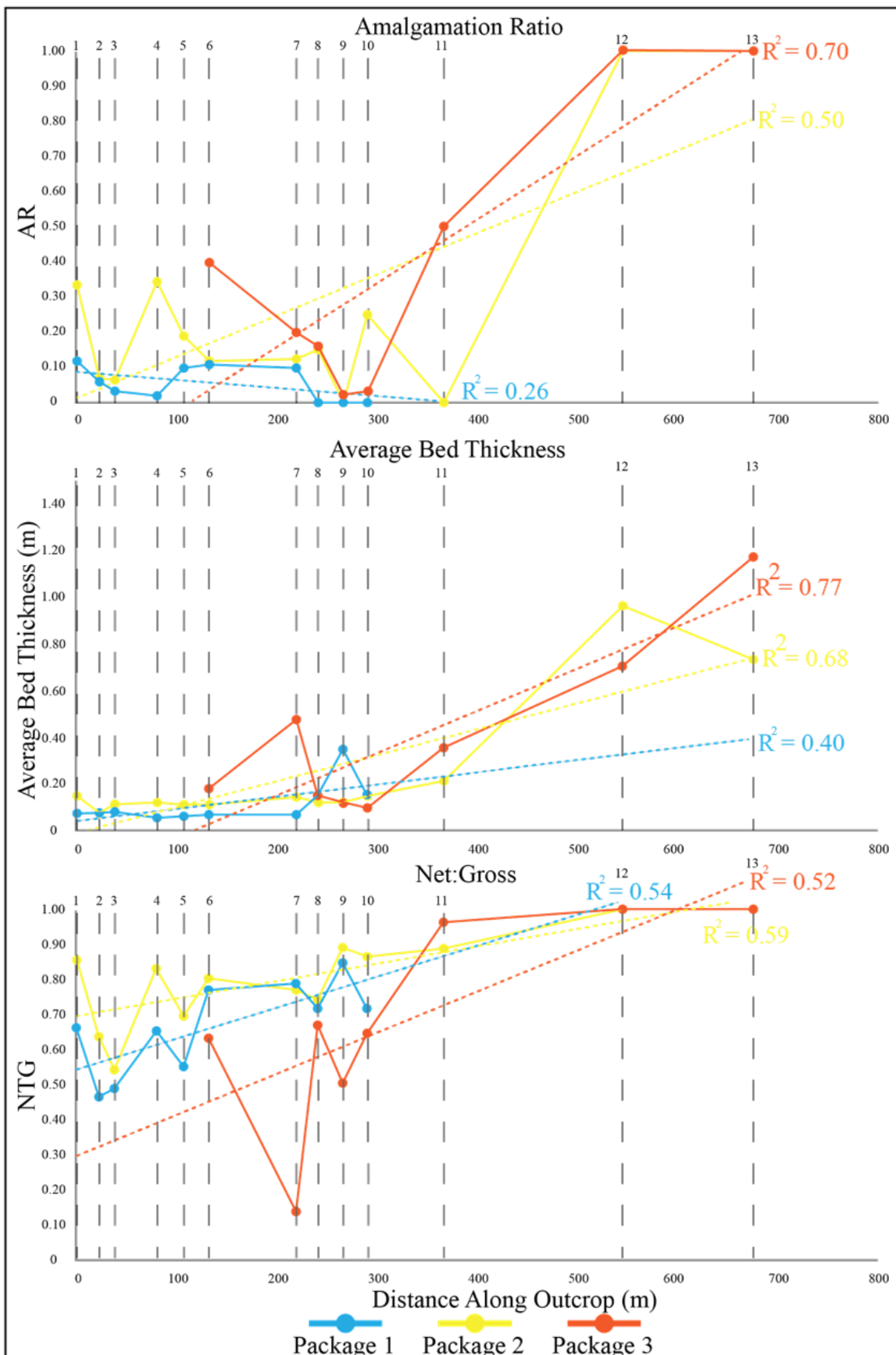
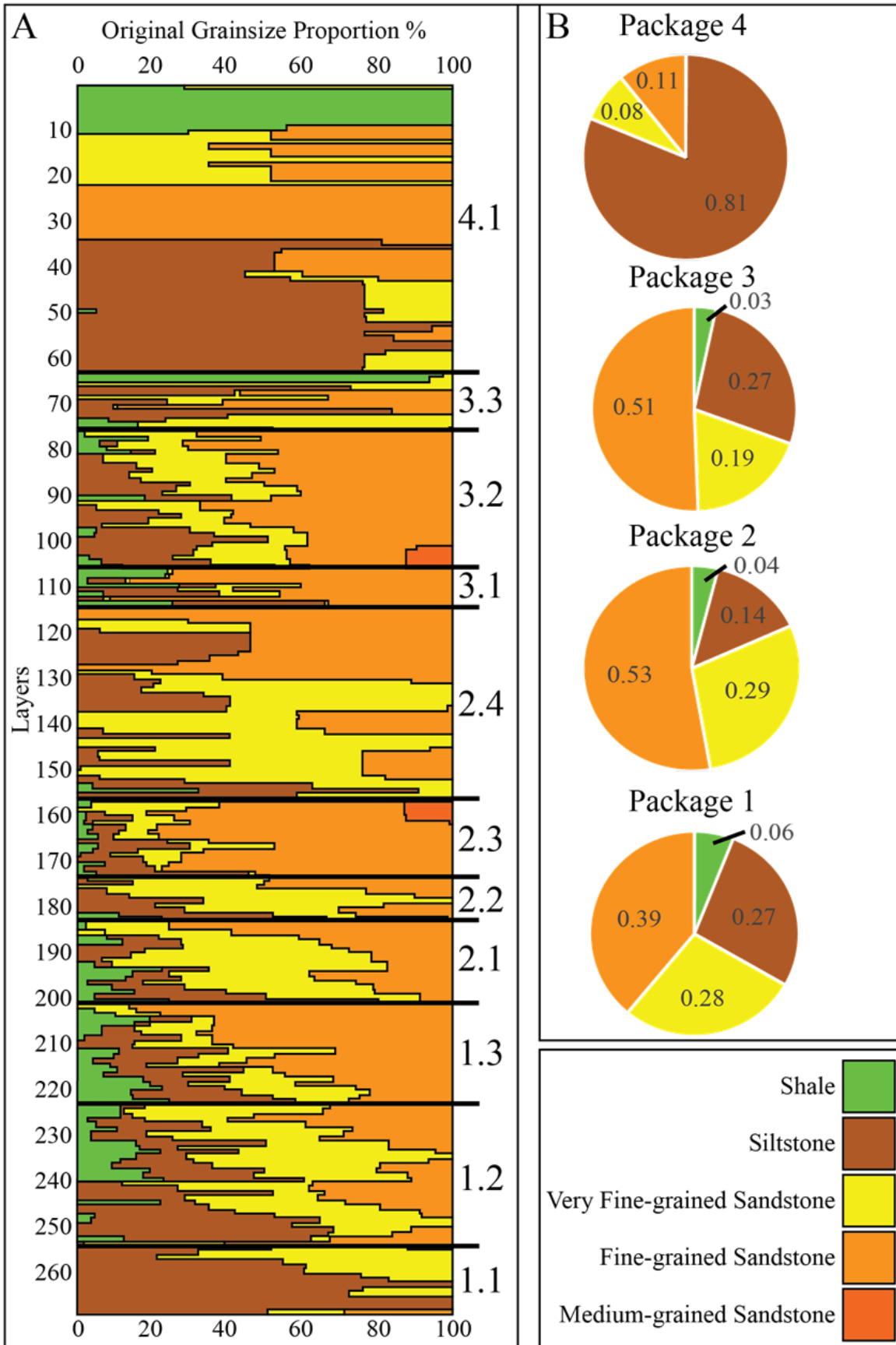


Figure 14. Vertical grain size trend

Left) Grain size proportion curve of bayhead delta stories. In general, grain size increases up-section until the top of story 3.3, and then abruptly declines in the abandoned channel fill of story 4.1. Right) Pie charts of package lithologies showing the percentage of each grain size that composes the packages. P1, proximal prodelta, is dominated by siltstone and very fine sandstone. P2 and P3 show very similar grain size percentages, both being delta front facies. These packages show the highest NTG of the packages, with high percentages of very fine and fine sandstones. Siltstone with minor amounts of sandstone dominates P4 (abandoned channel fill).



## DISCUSSION

Outcropping paralic facies assemblages in the John Henry Member of Tibbet Canyon offer a case study of an estuarine fill succession. In this discussion, detailed and statistical facies analysis of the bayhead delta in Tibbet Canyon is compared to a study of similar lithofacies from tide-influenced point bar deposits, to investigate implications for IHS-dominated hydrocarbon reservoirs. Second, a depositional model addresses the three-phase, transgressive-regressive stratigraphic evolution of Tibbet Canyon estuarine strata. Finally, correlations across ~20 km between Tibbet Canyon and previous John Henry Member study areas in Bull Canyon and Kelly Grade are addressed, as well as possible regional sequence stratigraphic implications for estuarine deposits in the southern Kaiparowits Plateau.

### **Bayhead Delta IHS Characterization**

The model created for the bayhead delta of interest in Tibbet Canyon (Fig. 15) and a similar model made from a tide-influenced point bar of Durkin et al. (in press) are used in this study to compare sedimentologic trends in both of these IHS-dominated deposits (Fig. 16). Tide-influenced point bars of Durkin et al. (in press) are from south central Alberta, in Upper Cretaceous (Campanian-Maastrichtian) meander belt deposits of the Horseshoe Canyon Formation. The Horseshoe Canyon Formation and the Lower Cretaceous McMurray Formation were deposited in similar settings (tide-influenced

fluvio-estuarine channels) (Rahmani, 1988, 1989; Musial et al., 2012). Although the Horseshoe Canyon Formation is not a SAGD tar sand reservoir target, outcrops have excellent 3D control, offering insight into meander bend evolution that can be applied to subsurface reservoirs, such as the McMurray Formation. Channel deposits of the Horseshoe Canyon Formation model are 12-16 m thick and extend for 600 m laterally, compared to the 8-10 m thick and 500 m laterally extensive bayhead delta in Tibbet Canyon, Utah. For comparison, facies mapped by Durkin et al. (in press) were converted to grain size equivalents based on dominant lithology, specifically, where Durkin et al.'s (in press) fine-grained sandstone remains fine-grained sandstone, siltstone with sandstone and organic interbeds becomes siltstone, and organic-rich mudstone becomes mudstone.

Overall grain size trends of the Tibbet Canyon bayhead delta progradational packages (P1-P4) indicate that P1 and P2 have a coarsening-upward grain size trend (Fig. 16). P3 and P4 show overall fining-upward trends. P1, P2, and P3 have individual stories that show coarsening-upward trends. P2 and P3 are both representative of delta front facies. However, P3 has an overall finer grain size than P2. This could be due to a decrease in fluvial sediment discharge, a local avulsion, etc. P4 represents abandoned channel fill, with a fining-upward grain size trend, and in Tibbet Canyon, this package marks the final stage of delta occupation.

Individual story trends show relative changes in grain size (Fig. 16). The trajectory of the trends within each story may indicate relative accommodation versus sediment supply for this part of the delta. The majority of stories show systematic increases in grain size, which probably reflect normal delta deposition (Bhattacharya, 2006; Ahmed et al., 2014). Stories 2.3, 3.2, and 3.3 show a steeper-angle grain size

trajectory, and therefore appear more aggradational than progradational (Fig. 16). These aggradational events could reflect a combination of increased fluvial discharge accompanied by an increase in grain transport. Increased discharge may occur seasonally or might be caused by a single storm event (Nichol et al., 1997). Bayhead deltas are deposited in shallow water depths (<2 m) (Simms and Rodriguez, 2014) and have low gradients down-dip (Rodriguez et al., 2010), making them sensitive to small changes in local accommodation. Thus, seasonal changes in discharge and central bay water depth could have a noticeable impact on grain size trends.

Overall trends from the tide-influenced fluvial point bar (Fig. 16) show three fining-upward grain size trends, which is consistent with proposed trends for IHS point bars (Thomas et al., 1987). Fining-upward facies associations of point bar deposits in the Horseshoe Canyon Formation are 10-12 m thick and are composed of lateral accretion packages that range from 1-5 m thick and tens of meters across in the depositional dip direction. Each overall grain size trend likely corresponds to point bar rotation and intra-point bar erosion (Durkin et al., in press). Taking the proportion curve as a whole into account, there is a general fining-upward trend from fine-grained sandstone at the base to siltstone and mudstone facies at the top.

Grain size proportion curves for the bayhead delta and the tide-influenced point bar display inverse trends (Fig. 16). The base of the bayhead delta to the top of story 3.3 generally coarsens upward. Even though P3 shows a slight decrease in grain size, this is negligible compared to the decrease in grain size experienced by the abandoned channel of P4. From the base of the point bar to the top of story 16, the point bar shows a fining-upward trend. Story 17 represents abandoned channel fill, similar to story 4.1 in the

bayhead delta. An abrupt decrease in NTG marks the base of 4.1. The similarity of the trends between bayhead deltas and tide-influenced point bars suggests that findings from reservoir models of IHS point bars can be informative as to how bayhead delta reservoirs will behave in the subsurface.

Considering the other outcrop statistics (average bed thickness, AR, and NTG), it is possible to determine where the most prospective reservoir facies exist in the bayhead delta. Based on the graphs, NTG, average bed thickness, and AR are highest at >500 m from the origin of the bayhead delta exposure, along the northern section of the outcrop. Reservoir quality for prograding deltas is expected to increase upward and toward the sandstone body axis (White et al., 2004). Because AR is high in this area, shale drapes are less likely to compartmentalize the reservoir. NTG is high, with very fine- and fine-grained sandstone beds dominating. Average bed thickness further reduces the risk for reservoir compartmentalization or poor connectivity. The fewer beds that exist within a given reservoir interval, the more likely those beds will maintain flow communication. Positions <500 m from the origin of the outcrop are not ideal reservoir candidates due to their lower NTG, average bed thickness, and AR. They are depositionally up-dip and off-axis from the main sandstone deposition. Therefore, reservoirs in this part of the bayhead delta are poor, being too fine-grained, compartmentalized, and isolated by shale drapes. However, some sandstone beds might still be in communication with beds along the main channel axis.

Through statistical analysis, it appears that bayhead deltas and tide-influenced point bars have predictable facies trends and are both descriptively and quantitatively IHS deposits. The fact that they display similar accretionary, inclined bed sets and draping,

yet opposite trends in grain size, NTG, average bed thickness, and AR, is useful for reservoir modeling purposes. These differing trends are a result of the depositional nature of delta and point bars, whereby deltas prograde and accrete parallel to flow direction and point bars accrete perpendicular to flow direction.

### **Tibbet Canyon Estuarine Evolution**

Strata cropping out within Tibbet Canyon at RPTC-2 (Fig. 4) show characteristics of a mixed-energy estuary in the basal deposits, becoming more wave-dominated upsection. This ~65-m-thick fill pattern (Fig. 17) captures the development of transgressive tidal bars at the base of the section (T<sub>1</sub>, LA 1.1), transgressive-regressive central basin fill (T<sub>2</sub>, LA 1.2), and regressive bayhead delta overlain by regressive coastal plain deposits (T<sub>3</sub>, LA 1.3). The change in facies architecture thus records a shift from mixed-energy to wave-dominated estuary settings.

Identification of inner estuary tidal bars deposited during T<sub>1</sub> (Fig. 17) is a key factor in interpreting the Tibbet Canyon area estuary as a mixed-energy system. The basal section of the John Henry Member measured at RPTC-2 preserves tidal bars of LA 1.1 overlying the Calico Bed. The top of the Calico Bed itself is burrowed by traces of the *Glossifungites* ichnofacies, which is representative of subaerial exposure followed by subsequent marine incursion and colonization during transgression (MacEachern et al., 1992). Therefore, the basal tidal bars are likely transgressive deposits. These types of bars form by tidal currents modifying fluvial-derived sediments of a bayhead delta, thereby giving it a tide-dominated delta morphology. Inner estuary tidal bars are not to be confused with more commonly considered “elongate tidal bars” which form at the mouth



of tide-dominated estuaries (Dalrymple et al., 2012; Dalrymple and Choi, 2007) and have relative good sorting and coarse sandstone grain sizes as well as a general lack of mud drapes (Plink-Björklund, 2008). Tidal bars are encased over tens of meters laterally by heterolithic fine-grained deposits interpreted as bay fill. The same basal interval ~1 km to the east, continuing several km to the mouth of Tibbet Canyon, is fluvial.

Stratigraphically above the tidal bars are horizontally bedded, brackish, fine-grained sediments including mudstone, siltstone, sandstone, and coal. No abrupt bounding surfaces exist, but a decrease in grain size and a lack of sigmoidal tidal bars marks the transition, with the central bay (LA 1.2) forming due to a decrease in depositional energy. The bay fill is overlying the tidal bars, which are positionally down-dip of the tidal bar-modified bayhead delta deposits of LA 1.1. This likely represents continued transgression and deposition of more basinward bay fill deposits stratigraphically above the tidal bars. Also, with the bayhead delta of LA 1.3 above the bay fill, which marks regressive fill into the estuary (Aschoff, 2009), the maximum transgressive surface likely exists within the bay fill and marks the transgressive-to-regressive turnaround (Fig. 17C).

Above the bay fill, a bayhead delta is deposited ( $T_3$ , Fig. 17), showing fluvial-dominated characteristics common to wave-dominated estuaries (Steel et al., 2012; Joeckel and Korus, 2012; Plink-Björklund, 2008; Dalrymple et al., 1992). Heterolithic bay fill deposits exist laterally to the bayhead delta and coastal plain fluvial deposits overlie the delta itself. At about the same stratigraphic level as the bayhead delta, IHS point bar deposits have been interpreted ~3 km away at the mouth of Tibbet Canyon (Shanley et al., 1992). The interpretation of IHS bayhead deltas and IHS point bars is

further complicated because they can exist within the same stratigraphic interval.

Bayhead delta deposits (LA 1.3) are progradational, fluvial-dominated features which mark the transition from transgressive to regressive deposition (Aschoff, 2009). In wave-dominated estuaries, relative fluvial energy is greater than tidal energy, creating fluvial-dominated delta characteristics. However, tidal and brackish indicators are still present (e.g., double mud drapes, flaser bedding, brackish trace fossils). In mixed-energy estuaries, increased tidal energy in the inner estuary causes winnowing and remobilization of fluvial sediments supplied to the bayhead delta. Tidal action leads to the formation of tidal bars within the estuary, instead of a bayhead delta (Fenies and Tastet, 1998; Billy et al., 2012; Chaumillon et al., 2013). The presence of mixed-energy estuary tidal bars (LA 1.1) at the base of the sequence and wave-dominated bayhead delta deposits (LA 1.3) at the top of sequence, suggests a relative decrease in tidal processes over the ~65 m-thick estuary succession.

One likely scenario explaining the process regime change and decreasing tidal energy from mixed-energy to wave-dominated estuary could be a change in the estuary morphology, thereby interfering with tidal resonance and decreasing tidal wave amplification. During the initial transgression and deposition of the basal tidal bars, the estuary was likely more funnel-shaped, based on the geometries predicted by estuary facies models (Dalrymple et al., 1992; Dalrymple, 2006). With continued transgression, tidal ravinement processes could have eroded the valley walls, thereby widening the estuary (Willis, 1997; Willis and Gabel, 2003; Li and Bhattacharya, 2013; Chentnik et al., in press). Decreased estuary constriction would have caused the tidal range to decrease and the estuary would be more wave-dominated (Plink-Björklund, 2008). Continued

deposition in the estuary would have experienced decreased tidal energy due to a reduction in funnel constriction and dampening of tidal amplification.

Another hypothesis to explain changing tidal energy in the estuary is the formation of barrier islands across the mouth of the estuary (Dalrymple et al., 1992; Roy, 1994; Plink-Björklund, 2008). During the first stages of the transgression, the estuary mouth may have been more open, allowing for a higher degree of tidal energy to penetrate into the estuary (Allen and Posamentier, 1993; Allen, 1991; Cattaneo and Steel, 2003). However, longshore drift accounts for a significant component of sediment deposited in the shorefaces of the Straight Cliffs Formation along the eastern edge of the Kaiparowits Plateau (Allen and Johnson, 2010a; Szwarc et al., in press). In addition, barrier islands systems occur in Buck Hollow (Mulhern et al., 2014) and Left Hand Collet (Dooling, 2013). Therefore, it is reasonable to suggest that longshore drift could have supplied sufficient sediment across the estuary mouth, creating a barrier island or spit. Barrier islands decrease tidal energy within estuaries by restricting the estuary mouth and dissipating tidal power.

### **Stratigraphic Correlations**

Plateau-wide correlations within the John Henry Member are difficult due to complex stratigraphy and lack of ash beds and other clear time datums. This discussion mainly focuses on correlations with the fluvial and tidal deposits of the southern margin of the plateau (Shanley et al., 1992; Gallin et al., 2010; Gooley, 2010; Pettinga, 2013). This study is the first clear documentation of an estuary formed in the lower John Henry Member of the Tippet Canyon area. Interpretations made by Shanley et al. (1992)

indicate tidal influence of fluvial deposits at the mouth of Tippet Canyon (RPTC-5, Fig. 3). However, just a few km to the west, a full estuarine succession is observed, nestled in amongst the surrounding fluvial strata. Although a valley edge is explicitly defined, deposition of estuarine deposits typically occurs within a flooded river valley. Therefore, the fluvial sections in the eastern mouth of Tippet Canyon might predate the basal tidal bar measured at RPTC-2, which would place the eastern valley edge between RPTC-2 and RPTC-5 (Fig. 3). Alternatively, these fluvial deposits might be lateral fluvial equivalents to the tidal bars, although this is unlikely (Boyd et al., 2006). Regardless, this study shows that marine influence extends further west in the plateau than previously recognized, up depositional dip from the coeval shoreline.

#### *Regional Marker Beds and Datums*

The Calico Bed marks the top of the Smoky Hollow Member and is a regionally extensive gravel sheet comprised of laterally and vertically amalgamated fluvial channels that record deposition during a period of low accommodation relative to sediment supply (Bobb, 1991; Shanley and McCabe, 1991). Marine traces of the *Glossifungites* ichnofacies are also preserved at the top of the Calico Bed.

The Drip Tank Member is the uppermost of the Straight Cliffs Formation, consisting of ~20 m of coarse-grained fluvial sandstone and channel lag conglomerates in Tippet Canyon. Channel bodies within the Drip Tank Member amalgamate both vertically and laterally, and floodplain deposits are rare. Shanley and McCabe (1991) mark the base of the Drip Tank Member as a sequence boundary, although recent studies suggest that the sequence boundary is near the middle of the Drip Tank Member (Lawton

et al., 2003; Schellenbach, 2013; Lawton et al., 2014).

### *Up-Dip Correlations*

Studies focusing on fluvial architecture at Rock House Cove and Bull Canyon (Fig. 1) (Gooley et al., in press), 25 and 15 km NW of the main Tibbet Canyon section, respectively, document trends in average channel widths, grain size, net-to-gross, channel clustering, channel stacking, and paleoflow. At these locations, fluvial strata in the lower John Henry Member (0-27 m above the Calico Bed) display an up-section decrease in average grain size accompanied by a reduction in channel widths, lateral and vertical channel amalgamation, and net-to-gross. The lower John Henry Member also displays tide-influenced fluvial and coastal plain mires in the form of localized IHS deposits. Laterally restricted channel belts with abundant coals and floodplain mudstones comprise the middle John Henry Member (27-90 m above the Calico Bed). Paleocurrent indicators throughout the John Henry Member indicate east and northeast-directed paleoflow (Fig. 18). The upper John Henry Member (90-215 m above the Calico Bed) exhibits an up-section increase in average grain size, correlative with an increase in channel belt width, amalgamation, and net-to-gross (Fig. 18). This change in fluvial channel belt morphology might relate to thrust belt activity in the Paxton thrust sheet and subsequent progradation of distributive fluvial systems draining the Sevier thrust belt across the Kaiparowits Plateau (Szwarc et al., 2015).

Tibbet Canyon displays a similar stratigraphic and architectural pattern. Basal deposits in Tibbet Canyon are composed of estuary tidal bars overlain by transgressive central basin fill fines (LAs 1.1 and 1.2). Therefore, there is an initial decrease in grain

size coincident with the transgression of the estuary. Above the bay fill is the bayhead delta of LA 1.3 overlain by fluvial deposits. Fluvial deposits display coarsening-upward, increase in channel belt complexity and lateral extent, and a lack of tidal signatures, like the upper John Henry Member deposits of Bull Canyon and Rock House Cove. When comparing tidal influence and grain size trends from Bull Canyon/Rock House Cove to Tibbet Canyon, it seems likely that deposition of the lower to Middle John Henry Member is associated with the emplacement of the Tibbet Canyon estuary (Fig. 18). This is not meant to be a lithostratigraphic correlation, but rather an identification of the lateral facies and depositional environment relationships one would expect to find for time-correlative intervals.

#### *Down-Dip Correlations*

Gallin et al. (2010) detailed paralic stratigraphy of the John Henry Member in the Kelly Grade area, ~10 km east of Tibbet Canyon (Fig. 1; Fig. 18). Measured sections record strata from the top of the Calico Bed to the base of the Drip Tank Member. Above the Calico Bed, the lower John Henry Member (0-40 m) consists of tide-influenced fluvial channel belts and coastal plain coal mires (Gallin et al., 2010), as well as isolated trace fossil evidence of marine influence. The main evidence for marine influence occurs in the middle John Henry Member (40-115 m above the Calico Bed) at Kelly Grade, with bayhead deltas, carbonaceous estuarine and lagoonal bay fill mudstone, isolated distributary channels, laterally restricted channels, and laterally restricted channel belts. Finally, the upper John Henry Member (115-225 m above the Calico Bed) is composed of laterally extensive channels belts, channel belt complexes, and floodplain mudstones,

generally lacking indication of tidal influence (Gallin et al., 2010). Comparing maximum tidal influence and depositional environments, the middle John Henry Member of Gallin et al. (2010) and FA-1 are most similar (Fig. 18). Both of the facies associations have bayhead delta deposits, which, as discussed, are significant stratigraphic and paleoenvironment markers. Therefore, tide-influenced fluvial channel belts in the lower John Henry Member of Kelly Grade likely correspond to the fluvial-dominated channels in the western Tibet Canyon lower John Henry Member (Fig. 18).

### *Broader Stratigraphic Implications*

Recent studies focusing on the shallow marine architecture of the John Henry Member of the eastern plateau (Rogers Canyon, Fig. 1) identified multiple transgressive-regressive shoreface cycles (Allen and Johnson, 2010a, 2011, 2010b) (Fig. 18), corresponding to the main “A-G” shoreface units described by Peterson (1969b). Allen and Johnson (Allen and Johnson, 2010a, 2011, 2010b) determined that shorefaces “A” and “B” are progradational, shorefaces “C”, “D”, and “E” are retrogradational, and shorefaces “F”/“G” are aggradational to retrogradational. Furthermore, they recognized that a major, ~17 km basinward shift in the shoreline occurred between the “B” and “C” shorefaces, more than twice the apparent basinward shift recorded from the “A” to “B” shoreface packages. This suggests that the “A-B-C” shoreface intervals are part of a forced regression. Other studies corroborate these trends in shoreline stacking patterns (Hettinger, 1995; Dooling et al., 2012; Mulhern et al., 2014; Chentnik et al., in press).

At Main Canyon (Fig. 1), Chentnik et al. (in press) observe a major subaerial unconformity, which occurs within the “C” interval, with southwest- to northeast-

trending incisions at the top of the “B” shoreface, which in places remove this ~25-m-thick shoreface interval entirely. This is a compound surface representing subaerial unconformity later modified by tidal ravinement, and Chentnik et al. (in press) propose calling it the “lower John Henry Member sequence boundary,” replacing the “A” sequence boundary of Shanley and McCabe (1991). Results from Tibbet Canyon, as presented here, suggest that the lower John Henry Member sequence boundary might extend to the southern plateau.

Initial John Henry Member deposition in much of Tibbet Canyon was dominated by fluvial deposition, which likely occurred during net progradation of the “A-B-C” shoreface intervals. These fluvial deposits in the lower John Henry Member of Tibbet Canyon probably correlate to tide-influenced fluvial and coastal plain deposits in Kelly Grade (Gallin et al., 2010) (Fig. 18). However, in places such as the main Tibbet Canyon section (RPTC 2; Fig. 3), the Calico Bed is overlain, and locally entirely removed by estuarine tidal bars of the lowermost John Henry Member. We suggest this unconformable facies relationship, as well as the Calico Bed *Glossifungites* ichnofacies, might be the local expression of a combined subaerial unconformity and transgressive ravinement surface in the lower John Henry Member, specifically associated with the retrogradational shoreface stacking patterns in the “C-D-E” intervals. Subsequently, the estuary was filled and then overlapped by a prograding coastal plain succession in the upper John Henry Member (Gooley et al., in press).



Figure 15. Bayhead delta outcrop package cross section

South to north cross section, from A to A', of bayhead delta outcrop showing the distribution of packages and their orientation in space. The cross section was created using zone modeling with the measured section and story surfaces as inputs. Distances measured in meters. Note the truncation and lenticular nature of packages in delta front facies as well as the significant scour caused by the abandoned channel. Package surfaces created with this model served as the guide for model layering used in generating the grain size proportion curves. Example of package layers shown with Story 1.1 of package 1.

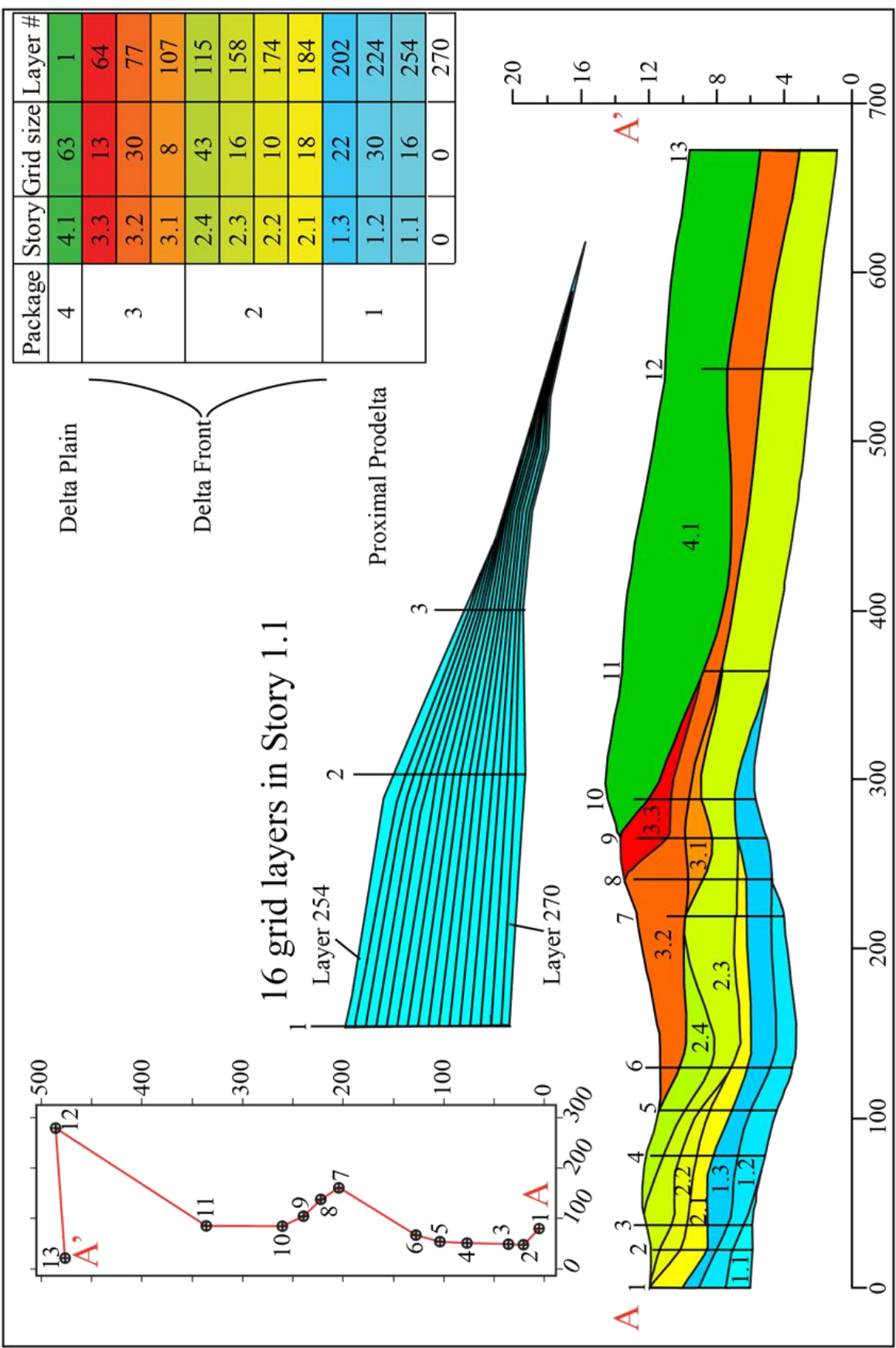


Figure 16. Grain size proportion curve comparison of a bayhead delta and tide-influenced point bar

Left) Grain size proportion curve of bayhead delta in this study. Overall grain size trends indicate that P1 and P2 are coarsening-upward, while P3 and P4 show overall fining-upward trends. As a whole, the bayhead delta coarsens upward to the top of P3 and then abruptly fines in the abandoned channel fill of P4.

Right) Grain size proportion curve of a tide-influenced bayhead delta from the Campanian-Maastrichtian Horseshoe Canyon Formation of Alberta, Canada (Durkin et al., in press). Overall trends from the tide-influenced fluvial point bar show three fining-upward grain size trends and an overall fining-upward trend, which is consistent with proposed trends for IHS point bars (Thomas et al., 1987).

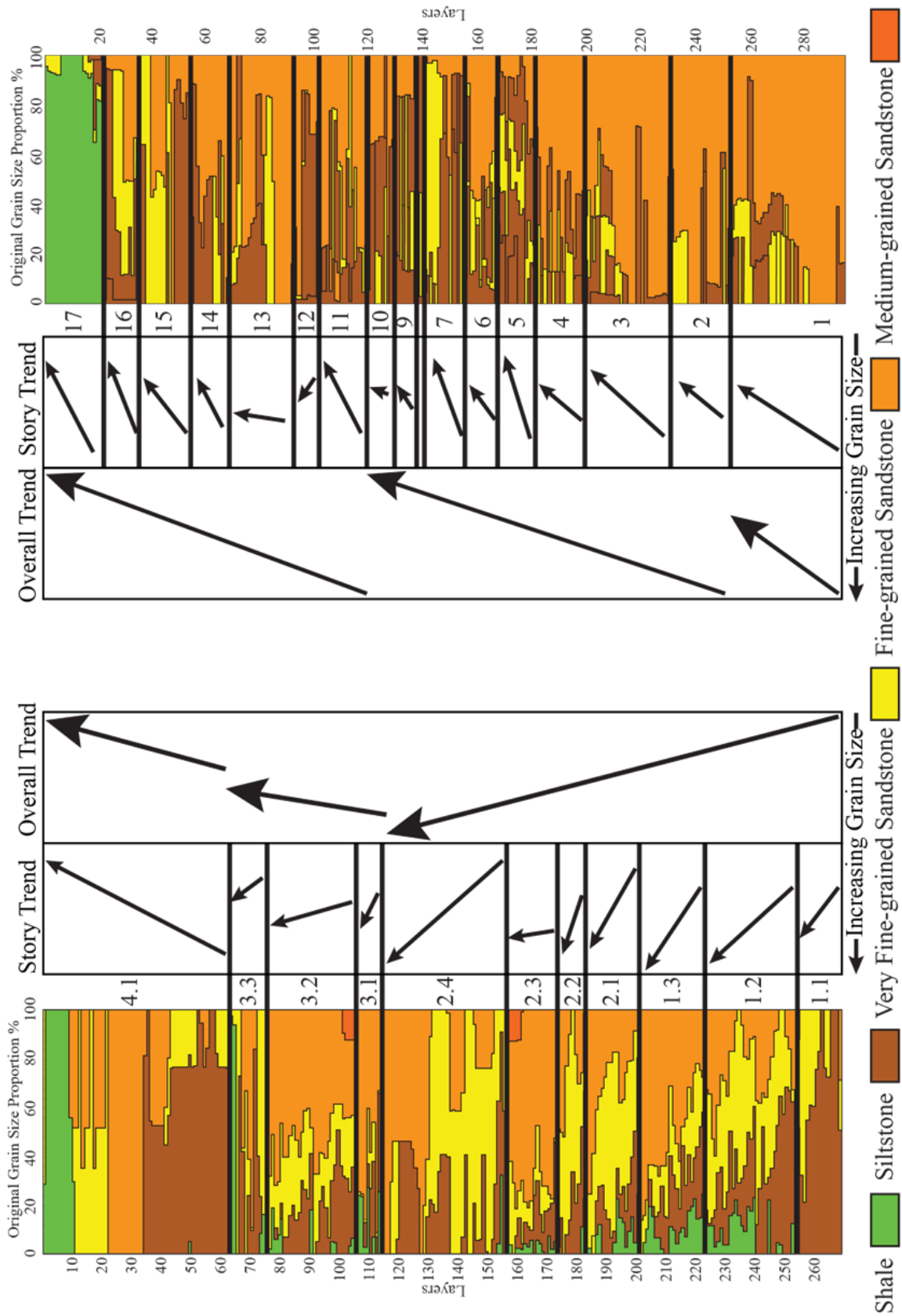


Figure 17. Depositional model and estuary evolution of Tibbet Canyon strata at RPTC-2

Left) Depositional model explaining the stratigraphic evolution of Tibbet Canyon at RPTC-2 (Fig. 4). The model scale represents actual dimensions and paleogeography responsible for the deposition in Tibbet Canyon. T<sub>1</sub> shows deposition of mixed-energy estuarine tidal bars of LA 1.1. T<sub>2</sub> shows crevasse channel deposits amongst bay fill deposits of LA 1.2. T<sub>3</sub> represents those final stages of progradation of a bayhead delta into a wave-dominated estuary.

Right, Top) Plan view schematic estuary evolution illustrating the change from mixed-energy (T<sub>1</sub>) to wave-dominated (T<sub>3</sub>) estuary. Sequence shows a widening of the estuary funnel, decreasing coastal embayment, and barrier island migration across the estuary mouth. Each of these changes may explain the decrease in relative tidal influence the estuary experienced during time of deposition.

Right, Bottom) Schematic stratigraphic cross section of measured section RPTC-2 showing transgression of mixed-energy estuary with deposition of tidal bars and bay fill, followed by regression and progradation of a fluvial-dominated bayhead delta of a wave-dominated estuary.

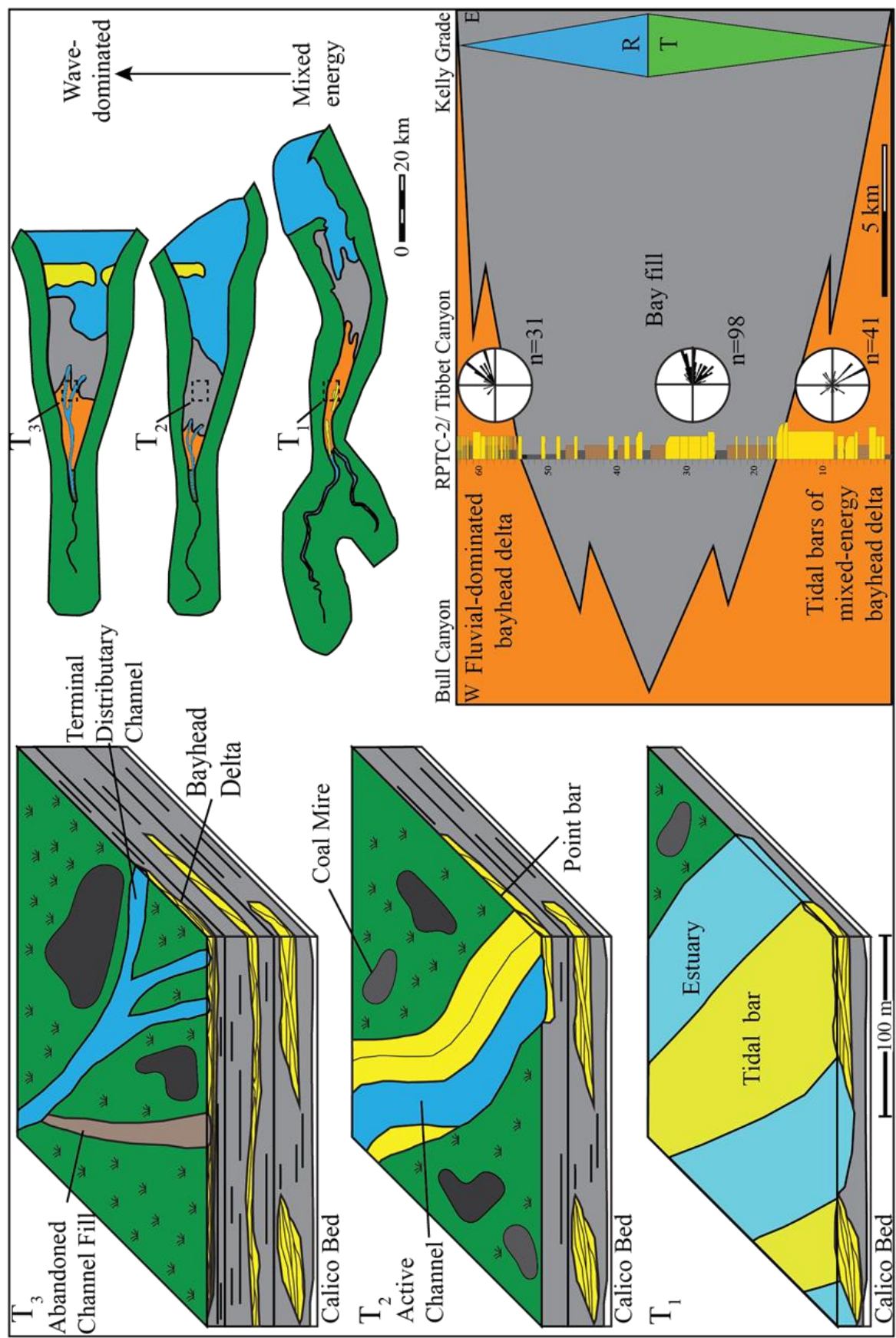
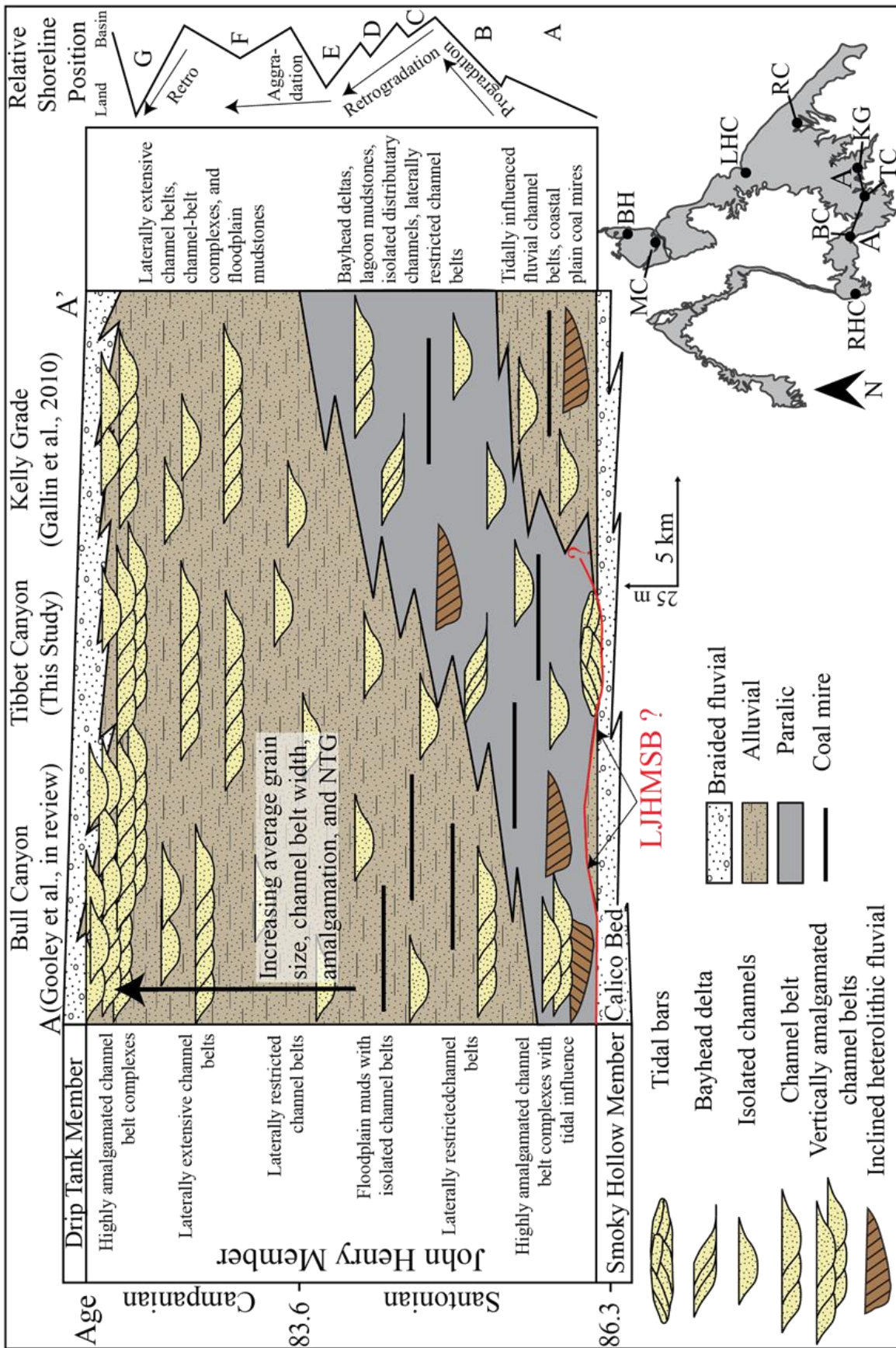


Figure 18. Southern Kaiparowits Plateau stratigraphic correlation

Schematic cross section correlation of the Straight Cliff Formation John Henry Member in the southern portion of Kaiparowits Plateau. Line of section intersects deposits of Bull Canyon, Tibbet Canyon, and Kelly Grade (A to A' on the inset where gray shading represent outcrops of the Straight Cliffs Formation) and shows proposed correlation of the southern plateau incorporating the lower John Henry Member sequence boundary (LJHMSB). This sequence stratigraphic surface corresponds to regression and subsequent transgression that occurred between the "B" and "C" shorefaces. The LJHMSB may be responsible for removal of "A" and "B" shoreface equivalent deposits in Bull Canyon and Tibbet Canyon, and deposition of transgressive estuarine deposits in the southern Kaiparowits Plateau. Abbreviations: BH-Buck Hollow, MC-Main Canyon, LHC-Left Hand Collet, RC-Rogers Canyon, KG-Kelly Grade, TC-Tibbet Canyon, BC-Bull Canyon, RHC-Rock House Cove.







## CONCLUSION

Three facies associations are preserved within the John Henry Member at Tibbet Canyon: estuary fill, tide-influenced coastal plain, and coastal plain. Estuary depositional architectures show a relative decrease in tidal regime over ~65 m of vertical section, and are interpreted as a shift from a mixed-energy to a wave-dominated estuarine setting. Additionally, Tibbet Canyon estuarine strata provide an outcrop-based case study for transgressive-to-regressive process-regime change models.

Statistical analysis and outcrop modeling quantitatively characterize a bayhead delta reservoir analog, and provide insight into the development of IHS deposits. Comparison between tide-influenced point bars and bayhead deltas indicate that they have similar architectures (accretionary and inclined bed sets with mud drapes), yet inversely related sedimentologic trends (grain size, NTG, average bed thickness, and AR). Stories and packages defined in the bayhead delta coarsen upward until they are capped by abandoned channel fill mudstone. The highest quality reservoir targets are predicted to exist parallel to the delta progradational axis, where average grain size is coarsest, and NTG and AR are high. Inclined heterolithic point bars fine upward and have main reservoir targets perpendicular to the depositional trend, toward the base of the laterally accreting channel, where grain size is coarsest, and NTG and AR are highest. These patterns suggest that results from tide-influenced IHS point bar models can help

inform bayhead delta models, and vice versa. Understanding the effects of mudstone drapes on reservoir compartmentalization and fluid flow in IHS deposits is integral in managing these types of reservoirs and maximizing hydrocarbon production.

Relationships established in this study suggest that the lower John Henry Member estuarine deposits in Tibbet Canyon correlate up-dip to tide-influenced lower John Henry Member strata in Bull Canyon/Rock House Cove, and down-dip to lower and middle John Henry Member paralic strata in Kelly Grade. Correlations to previous stratigraphic studies in the southern Kaiparowits Plateau suggest that “A” and “B” shoreface-equivalent deposits are only locally present in Tibbet Canyon. These deposits may have been eroded by fluvial incision coincident with the basinward shift in shoreline during the “B” to “C” transition, which is here suggested to correlate with the lower John Henry Member sequence boundary recognized ~70 km north near Escalante, Utah. Estuarine and tidal strata were then deposited during the “C” to “E” relative shoreline transgression.

## REFERENCES

- Ahmed, S., Bhattacharya, J.P., Garza, D.E., and Li, Y., 2014, Facies architecture and stratigraphic evolution of a river-dominated delta front, Turonian Ferron Sandstone, Utah, U.S.A: *Journal of Sedimentary Research*, v. 84, p. 97–121, doi: 10.2110/jsr.2014.6.
- Ainsworth, R.B., Flint, S.S., and Howell, J.A., 2008, Predicting coastal depositional style: influence of basin morphology and accommodation to sediment supply ratio within a sequence-stratigraphic framework: Recent advances in models of shallow-marine stratigraphy: *SEPM Special Publication*, v. 90, p. 237–263.
- Ainsworth, R.B., Vakarelov, B.K., and Nanson, R.A., 2011, Dynamic spatial and temporal prediction of changes in depositional processes on clastic shorelines: toward improved subsurface uncertainty reduction and management: *AAPG Bulletin*, v. 95, p. 267–297, doi: 10.1306/06301010036.
- Allen, G.P., 1991, Sedimentary processes and facies in the Gironde estuary : a recent model for macrotidal estuarine systems, *in* Smith, D.G., Reinson, G.E., Zaitlin, B.A., and A., R.R. eds., *Clastic tidal sedimentology: Canadian Society of Petroleum Geologists Memoir 16*, p. 29–40.
- Allen, J.L., and Johnson, C.L., 2011, Architecture and formation of transgressive-regressive cycles in marginal marine strata of the John Henry Member, Straight Cliffs Formation, Upper Cretaceous of Southern Utah, USA: *Sedimentology*, v. 58, p. 1486–1513, doi: 10.1111/j.1365-3091.2010.01223.x.
- Allen, J.L., and Johnson, C.L., 2010a, Facies control on sandstone composition (and influence of statistical methods on interpretations) in the John Henry Member, Straight Cliffs Formation, Southern Utah, USA, *in* Carney, S.M. and Johnson, C.L. eds., *Sedimentary Geology, Salt Lake City, Utah Geological Association Publication*, p. 60–76.
- Allen, J.L., and Johnson, C.L., 2010b, Sedimentary facies, paleoenvironments and relative sea level changes in the John Henry Member, Cretaceous Straight Cliffs Formation, Southern Utah, USA, *in* Carney, S.M., Tabet, D.E., and Johnson, C.L. eds., *Geology of South-Central Utah, Salt Lake City, Utah Geological Association Publication*, p. 225–247.
- Allen, G.P., and Posamentier, H.W., 1993, Sequence stratigraphy and facies model of an incised valley fill: the Gironde Estuary, France: *SEPM Journal of Sedimentary Research*, v. Vol. 63, p. 378–391, doi: 10.1306/D4267B09-2B26-11D7-

8648000102C1865D.

- Allen, G.P., and Posamentier, H.W., 1994, Transgressive facies and sequence architecture in mixed tide- and wave-dominated incised valleys: example from the Gironde Estuary, France: *Journal of Sedimentary Petrology*, v. 63, p. 378–391.
- Armstrong, R.L., 1968, Sevier orogenic belt in Nevada and Utah: *Bulletin of the Geological Society of America*, v. 79, p. 429–458, doi: 10.1130/0016-7606(1968)79[429:SOBINA]2.0.CO;2.
- Aschoff, J.L., 2009, Recognition and Significance of Ancient Bayhead Delta Deposits: Uinta Basin, USA, *in RMS-SEPM: Luncheon Presentation Abstract*,.
- Banerjee, I., Kalkreuth, W., and Davies, E.H., 1996, Coal seam splits and transgressive-regressive coal couplets: a key to stratigraphy of high-frequency sequences: *Geology*, v. 24, p. 1001–1004, doi: 10.1130/0091-7613(1996)024<1001:CSSATR>2.3.CO;2.
- Bhattacharya, J.P., 2006, Deltas, *in* Posamentier, H.W. and Walker, R.G. eds., *Facies Models Revisited*, SEPM (Society for Sedimentary Geology), p. 237–292.
- Bhattacharya, J.P., 2003, Deltas and estuaries, *in* Middleton, G. ed., *Encyclopedia of Sediments and Sedimentary Rocks*, *Encyclopedia of Earth Science*, Dordrecht, Springer Netherlands, p. 145–152.
- Bhattacharya, J.P., and Giosan, L., 2003, Wave-influenced deltas: geomorphological implications for facies reconstruction: *Sedimentology*, v. 50, p. 187–210, doi: 10.1046/j.1365-3091.2003.00545.x.
- Biggs, R.B., 1967, The sediments of Chesapeake Bay, *in* Lauff, G.H. ed., *Estuaries*, AAAS, p. 239–260.
- Billy, J., Chaumillon, E., Féliès, H., and Poirier, C., 2012, Tidal and fluvial controls on the morphological evolution of a lobate estuarine tidal bar: The Plassac Tidal Bar in the Gironde Estuary (France): *Geomorphology*, v. 169-170, p. 86–97, doi: 10.1016/j.geomorph.2012.04.015.
- Bobb, M.C., 1991, The Calico Bed, Upper Cretaceous, southern Utah: a fluvial sheet deposit in the Western Interior foreland basin and its relationship to eustacy and tectonics: University of Colorado, 166 p.
- Boyd, R., Dalrymple, R.W., and Zaitlin, B.A., 1992, Classification of coastal sedimentary environments: *Sedimentary Geology*, v. 80, p. 139–150.
- Boyd, R., Dalrymple, R.W., and Zaitlin, B.A., 2006, Estuarine and incised-valley facies models, *in* Posamentier, H.W. and Walker, R.G. eds., *Facies Models Revisited*, SEPM (Society for Sedimentary Geology), p. 171–235.
- Bridge, J.S., 2003, *Rivers and floodplains: forms, processes, and the sedimentary record*: Oxford, United Kingdom, Blackwell Science Ltd, 504 p.
- Bridges, P.H., and Leeder, M.R., 1976, Sedimentary model for intertidal mudflat channels, with examples from the Solway Firth, Scotland: *Sedimentology*, v. 23, p.

533–552, doi: 10.1111/j.1365-3091.1976.tb00066.x.

- Broger, K.E.J., Syhlonyk, G.E., and Zaitlin, B.A., 1997, Glauconite Sandstone exploration: a case study from the Lake Newell Project, Southern Alberta: *Canadian Society of Petroleum Geologists Memoir*, v. 18, p. 140–168.
- Burton, D., and Wood, L.J., 2011, Quantitative shale characterization of the tidally influenced Sego Sandstone: *AAPG Bulletin*, v. 95, p. 1207–1226, doi: 10.1306/12081010119.
- Cambell, C. V., 1967, Lamina, laminaset, bed and bedset: *Sedimentology*, v. 8, p. 7–26, doi: 10.1111/j.1365-3091.1967.tb01301.x.
- Carrigy, M.A., 1971, Deltaic sedimentation in Athabasca tar sands: *AAPG Bulletin*, v. 55, p. 1155–1169.
- Cattaneo, A., and Steel, R.J., 2003, Transgressive deposits: a review of their variability: *Earth-Science Reviews*, v. 62, p. 187–228, doi: 10.1016/S0012-8252(02)00134-4.
- Chaumillon, E., Féliès, H., Billy, J., Breilh, J.F., and Richetti, H., 2013, Tidal and fluvial controls on the internal architecture and sedimentary facies of a lobate estuarine tidal bar (the Plassac Tidal Bar in the Gironde Estuary, France): *Marine Geology*, v. 346, p. 58–72, doi: 10.1016/j.margeo.2013.07.017.
- Chentnik, B.M., Johnson, C.L., Mulhern, J.S., and Stright, L., 2015, Valleys, estuaries, and lagoons: paleoenvironments and regressive-transgressive architecture of the Upper Cretaceous Straight Cliffs Formation: *Journal of Sedimentary Research*, v. 85, p. 1166–1196, doi: 10.2110/jsr.2015.70.
- Choi, K.S., Dalrymple, R.W., Chun, S.S., and Kim, S.P., 2004, Sedimentology of modern, inclined heterolithic stratification (IHS) in the macrotidal Han River Delta, Korea: *Journal of Sedimentary Research*, v. 74, p. 677–689, doi: 10.1306/030804740677.
- Coleman, J.M., and Prior, D.B., 1982, Sandstone depositional environments, *in* *AAPG Memoir*, AAPG Special Volumes, p. 139–178.
- Coleman, J.M., and Wright, L.D., 1975, Modern river deltas: variability of processes and sand units, *in* Broussard, M.L. ed., *Deltas, Models for Exploration*, Houston, TX, Houston Geological Society, p. 99–149.
- Coney, P.J., 1972, Cordilleran tectonics and North America plate motion: *American Journal of Science*, v. 272, p. 603–628, doi: 10.2475/ajs.272.7.603.
- Cummings, D.I., Arnott, R.W.C., and Hart, B.S., 2006, Tidal signatures in a shelf-margin delta: a product of shelf-edge embayment? *Geology*, v. 34, p. 249–252.
- Currie, B.S., 2002, Structural configuration of the Early Cretaceous Cordilleran foreland basin system and Sevier thrust belt, Utah and Colorado: *The Journal of Geology*, v. 110, p. 697–718, doi: 10.1086/342626.
- Dalrymple, R.W., 2006, Incised valleys in time and space; an introduction to the volume and an examination of the controls on valley formation and filling: *SEPM Special*

Publication, v. 85, p. 5–12.

- Dalrymple, R.W., and Choi, K., 2007, Morphologic and facies trends through the fluvial-marine transition in tide-dominated depositional systems: a schematic framework for environmental and sequence-stratigraphic interpretation: *Earth-Science Reviews*, v. 81, p. 135–174, doi: 10.1016/j.earscirev.2006.10.002.
- Dalrymple, R.W., Mackay, D.A., Ichaso, A.A., and Choi, K.S., 2012, Processes, morphodynamics, and facies of tide-dominated estuaries, *in* Davis, R.A. and Dalrymple, R.W. eds., *Principles of Tidal Sedimentology*, p. 79–107.
- Dalrymple, R.W., Zaitlin, B.A., and Boyd, R., 1992, Estuarine facies models; conceptual basis and stratigraphic implications: *Journal of Sedimentary Research*, v. 62, p. 1130–1146, doi: 10.1306/D4267A69-2B26-11D7-8648000102C1865D.
- DeCelles, P.G., and Coogan, J.C., 2006, Regional structure and kinematic history of the Sevier fold-and-thrust belt, central Utah: *Geological Society of America Bulletin*, v. 118, p. 841–864.
- Dickinson, W.R., 1974, Plate tectonics and sedimentation: *Tectonics and Sedimentation*, v. 22, p. 1–27, doi: 10.2110/pec.74.22.0001.
- Donaldson, A.C., Martin, R.H., and Kanes, W.H., 1970, Holocene Guadalupe Delta of the Texas Gulf Coast: Sedimentation, Modern and Ancient: *SEPM Special Publication*, v. 15, p. 107–137.
- Dooling, P.R., 2013, Tidal facies, stratigraphic architecture, and along-strike variability of a high energy, transgressive shoreline, Late Cretaceous, Kaiparowits Plateau, Southern Utah: University of Utah, 135 p.
- Dooling, P.R., Johnson, C.L., and Allen, J.L., 2012, Preservation and architecture of transgressive-regressive cycles in the Upper Cretaceous John Henry Member, of the Straight Cliffs Formation, Left Hand Collet, southern Utah, USA, *in* Abstracts with Program: AAPG Annual Convention and Exhibition 2012, Long Beach, CA,.
- Dreyer, T., Whitaker, M.F., Dexter, J., Flesche, H., and Larsen, E., 2005, From spit system to tide-dominated delta: integrated reservoir model of the Upper Jurassic Sognefjord Formation on the Troll West Field: *Petroleum Geology: North-West Europe and Global Perspectives - Proceedings of the 6th Petroleum Geology Conference*, p. 423–448, doi: 10.1144/0060423.
- Driese, S.G., Ludvigson, G.A., Roberts, J.A., Fowle, D.A., Gonzalez, L.A., Smith, J.J., Vulava, V.M., and McKay, L.D., 2010, Micromorphology and stable-isotope geochemistry of historical pedogenic siderite formed in PAH-contaminated alluvial clay soils, Tennessee, U.S.A.: *Journal of Sedimentary Research*, v. 80, p. 943–954, doi: 10.2110/jsr.2010.087.
- Durkin, P.R., Hubbard, S.M., Boyd, R.L., and Leckie, D.A., 2015, Stratigraphic expression of intra-point bar erosion and rotation: *Journal of Sedimentary Research*, v. 85, p. 1238–1257, doi: 10.2110/jsr.2015.78.
- Eaton, J.G., 1991, Introduction: tectonic setting along the margin of the Cretaceous

- Western Interior Seaway, southwestern Utah and northern Arizona, *in* Nations, J.D. and Eaton, J.G. eds., *Stratigraphy, depositional environments, and sedimentary tectonics of the western margin, Cretaceous Western Interior Seaway*, Geological Society of America, p. 1–8.
- Elliott, T., 1974, Intertributary bay sequences and their genesis: *Sedimentology*, v. 21, p. 611–622, doi: 10.1111/j.1365-3091.1974.tb01793.x.
- Feldman, H., Adereti, O., Ahmed, B., Ajibola, O., Alalade, B., Lopez, C., Sweet, M., Tsakma, J., Unomah, G., and Farre, J., 2013, Predicting large-scale reservoir architecture: application of data from shelf edge reservoirs in the eastern Niger Delta: *NAPE Bulletin*, v. 25, p. 52–80.
- Feldman, H.R., Fabijanic, J.M., Faulkner, B.L., and Rudolph, K.W., 2014, Lithofacies, parasequence stacking, and depositional architecture of wave- to tide-dominated shorelines in the Frontier Formation, Western Wyoming, U.S.A: *Journal of Sedimentary Research*, v. 84, p. 694–717, doi: 10.2110/jsr.2014.53.
- Fenies, H., de Resseguier, A., and Tastet, J., 1999, Intertidal clay-drape couplets (Gironde estuary, France): *Sedimentology*, v. 46, p. 1–15, doi: 10.1046/j.1365-3091.1999.00196.x.
- Fenies, H., and Tastet, J., 1998, Facies and architecture of an estuarine tidal bar (the Trompeloup bar, Gironde Estuary, SW France): *Marine Geology*, v. 150, p. 149–169, doi: 10.1016/S0025-3227(98)00059-0.
- Fletcher, S.D.T., Macauley, R. V., and Hubbard, S.M., 2011, Characterizing depositional elements of a deep water channel complex using quantitative metrics, Tres Pasos Formation, Southern Chile: 2011 CSPG CWLS Convention, p. 1–4.
- Fustic, M., Thurston, D., Adal, A.-D., Leckie, D.A., and Cadiou, D., 2013, Reservoir modeling by constraining stochastic simulation to deterministically interpreted three-dimensional geobodies: case study from Lower Cretaceous McMurray Formation, Long Lake Steam-Assisted Gravity Drainage Project, Northeast Alberta, Canada, *in* Hein, F.J., Leckie, D.A., Larter, S., and Suter, J. eds., *Heavy-Oil and Oil Sand Petroleum Systems in Alberta and Beyond: AAPG Studies in Geology 64*, AAPG, Canadian Heavy Oil Association and AAPG Energy Minerals Division, p. 1–39.
- Gallin, W.N., Johnson, C.L., and Allen, J.L., 2010, Fluvial and marginal marine architecture of the John Henry Member, Straight Cliffs Formation, Kelly Grade of the Kaiparowits Plateau, south-central Utah, *in* Carney, S.M., Tabet, D.E., and Johnson, C.L. eds., *Geology of South-Central Utah*, Salt Lake City, Utah Geological Association.
- Galloway, W.D., 1975, Process framework for describing the morphologic and stratigraphic evolution of deltaic depositional systems, *in* Broussard, M.L. ed., *Deltas: Models for Exploration*, Houston Geological Society, p. 86–98.
- Gooley, J.T., 2010, Alluvial architecture and predictive modeling of the late Cretaceous John Henry Member, Straight Cliffs Formation, southern Utah: University of Utah.

- Gooley, J.T., Johnson, C.L., and Pettinga, L., in press, Spatial and temporal variation of fluvial architecture within a prograding clastic wedge of the Late Cretaceous Western Interior Basin (Kaiparowits Plateau), USA: *Journal of Sedimentary Research*.
- Hancock, J.M., and Kauffman, E.G., 1979, The great transgressions of the Late Cretaceous: *Journal of the Geological Society*, v. 136, p. 175–186, doi: 10.1144/gsjgs.136.2.0175.
- Haq, B.U., Hardenbol, J., and Vail, P.R., 1987, Chronology of fluctuating sea levels since the Triassic: *Science (New York, N.Y.)*, v. 235, p. 1156–1167, doi: 10.1126/science.235.4793.1156.
- Hassanpour, M.M., Pyrcz, M.J., and Deutsch, C. V., 2013, Improved geostatistical models of inclined heterolithic strata for McMurray Formation, Alberta, Canada: *AAPG Bulletin*, v. 97, p. 1209–1224, doi: 10.1306/01021312054.
- Hettinger, R.D., 1995, Sedimentological descriptions and depositional interpretation, in sequence stratigraphic context, of two 300-meter cores from the Upper Cretaceous Straight Cliffs Formation, Kaiparowits Plateau, Kane County, Utah: U. S. Geological Survey, A1-A32 p.
- Holbrook, J.M., 1996, Complex fluvial response to low gradients at maximum regression: a genetic link between smooth sequence-boundary morphology and architecture of overlying sheet sandstone: *Journal of Sedimentary Research*, v. 66, p. 713–722, doi: 10.1306/D42683EC-2B26-11D7-8648000102C1865D.
- Horne, J.C., Ferm, J.C., and Caru, F.T., 1978, Depositional models in coal exploration and mine planning in Appalachian region: *AAPG Bulletin*, v. 62, p. 2379–2411, doi: 10.1306/C1EA5512-16C9-11D7-8645000102C1865D.
- Hubbard, S.M., Pemberton, S.G., Gingras, M.K., and Thomas, M.B., 2002, Variability in wave-dominated estuary sandstones: implications on subsurface reservoir development: *Bulletin of Canadian Petroleum Geology*, v. 50, p. 118–137, doi: 10.2113/50.1.118.
- Hubbard, S.M., Smith, D.G., Nielsen, H., Leckie, D.A., Fustic, M., Spencer, R.J., and Bloom, L., 2011, Seismic geomorphology and sedimentology of a tidally influenced river deposit, Lower Cretaceous Athabasca oil sands, Alberta, Canada: *AAPG Bulletin*, v. 95, p. 1123–1145, doi: 10.1306/12131010111.
- Jackson, R.G., 1981, Sedimentology of muddy fine-grained channel deposits in meandering streams of the American Middle West: *Journal of Sedimentary Research*, v. 51, p. 1169–1192, doi: 10.1306/212F7E5A-2B24-11D7-8648000102C1865D.
- Joeckel, R.M., and Korus, J.T., 2012, Bayhead delta interpretation of an upper Pennsylvanian sheetlike sandbody the broader understanding of transgressive deposits in cyclothems: *Sedimentary Geology*, v. 274-275, p. 22–37, doi: 10.1016/j.sedgeo.2012.07.002.



- Jordan, T.E., 1981, Thrust loads and foreland basin evolution, Cretaceous, western United States: *AAPG Bulletin*, v. 65, p. 2506–2520.
- Kauffman, E.G., 1977, Geological and biological overview: Western Interior Cretaceous basin: *Mountain Geologist*, v. 14, p. 75–99.
- Kirschbaum, B.M.A., and Hettinger, R.D., 2004, Facies analysis and sequence stratigraphic framework of Upper Campanian strata (Neslen and Mount Garfield Formations, Bluecastle Tongue of the Castlegate Sandstone, and Mancos Shale), Eastern Book Cliffs, Colorado and Utah: U.S. Department of the Interior, Report DDS-69-G,.
- Kraus, M.J., and Davies-Vollum, K.S., 2004, Mudrock-dominated fills formed in avulsion splay channels: examples from the Willwood Formation, Wyoming: *Sedimentology*, v. 51, p. 1127–1144, doi: 10.1111/j.1365-3091.2004.00664.x.
- Labrecque, P.A., Jensen, J.L., Hubbard, S.M., and Nielsen, H., 2011, Sedimentology and stratigraphic architecture of a point bar deposit, Lower Cretaceous McMurray Formation, Alberta, Canada: *Bulletin of Canadian Petroleum Geology*, v. 59, p. 147–171, doi: 10.2113/gscpgbull.59.2.147.
- Lawton, T.F., Pollock, S.L., and Robinson, R.A.J., 2003, Integrating sandstone petrology and nonmarine sequence stratigraphy: application to the Late Cretaceous Fluvial Systems of Southwestern Utah, U.S.A.: *Journal of Sedimentary Research*, v. 73, p. 389–406, doi: 10.1306/100702730389.
- Lawton, T.F., Schellenbach, W.L., and Nugent, A.E., 2014, Megafan and axial-river systems in the southern Cordilleran foreland basin: Drip Tank Member of Straight Cliffs Formation and adjacent strata, Southern Utah, USA: *Journal of Sedimentary Research*, v. 84, p. 407–434, doi: 10.2110/jsr.2014.33.
- Li, Y., and Bhattacharya, J.P., 2013, Facies-architecture study of a stepped, forced regressive compound incised valley in the Ferron Notom Delta, Southern Central Utah, U.S.A: *Journal of Sedimentary Research*, v. 83, p. 206–225, doi: 10.2110/jsr.2013.19.
- Liu, S., Nummedal, D., and Gurnis, M., 2014, Dynamic versus flexural controls of Late Cretaceous Western Interior Basin, USA: *Earth and Planetary Science Letters*, v. 389, p. 221–229, doi: 10.1016/j.epsl.2014.01.006.
- Liu, S., Nummedal, D., and Liu, L., 2011, Migration of dynamic subsidence across the Late Cretaceous United States Western Interior Basin in response to Farallon plate subduction: *Geology*, v. 39, p. 555–558, doi: 10.1130/G31692.1.
- MacEachern, J.A., Raychaudhuri, I., and Pemberton, S.G.G., 1992, Stratigraphic applications of the Glossifungites ichnofacies: delineating discontinuities in the rock record (S. G. Pemberton, Ed.): *Applications of Ichnology to Petroleum Exploration*, v. 82, p. 169–198.
- Mack, G.H., Leeder, M., Perez-Arlucea, M., and Bailey, B.D.J., 2003, Sedimentology, paleontology, and sequence stratigraphy of Early Permian Estuarine deposits, south-

central New Mexico, USA: *Palaios*, v. 18, p. 403–420, doi: 10.1669/0883-1351(2003)018<0403:SPASSO>2.0.CO;2.

- Madeleine Peijs-van Hilten, T., Good, R., and Zaitlin, B.A., 1998, Heterogeneity modeling and geopseudo upscaling applied to waterflood performance prediction of an incised valley reservoir: Countess YY Pool, Southern Alberta, Canada: *AAPG Bulletin*, v. 82, p. 2220–2245.
- Martinius, A.W., Kaas, I., Nss, A., Helgesen, G., Kjrefjord, J.M., and Leith, D.A., 2001, Sedimentology of the heterolithic and tide-dominated Tilje Formation (Early Jurassic, Halten Terrace, Offshore Mid-Norway): *Norwegian Petroleum Society Special Publications*, v. 10, p. 103–144, doi: 10.1016/S0928-8937(01)80011-4.
- Martinius, A.W., Ringrose, P.S., Brostrom, C., Elfenbein, C., Naess, A., and Ringas, J.E., 2005, Reservoir challenges of heterolithic tidal sandstone reservoirs in the Halten Terrace, mid-Norway: *Petroleum Geoscience*, v. 11, p. 3–16, doi: 10.1144/1354-079304-629.
- Martinsen, O.J., and Helland-Hansen, W., 1993, Sequence stratigraphy and facies model of an incised valley fill: The Gironde Estuary, France: *SEPM Journal of Sedimentary Research*, v. 63, p. 78–80, doi: 10.1306/D4267B09-2B26-11D7-8648000102C1865D.
- McLennan, J.A., and Deutsch, C. V, 2004, SAGD reservoir characterization using geostatistics: application to the Athabasca Oil Sands, Alberta, Canada: *Center for Computational Geostatistics Annual Report Papers*, p. 1–21.
- Miall, A.D., 1985a, Architectural-element analysis: A new method of facies analysis applied to fluvial deposits: *Earth-Science Reviews*, v. 22, p. 261–308, doi: 10.1016/0012-8252(85)90001-7.
- Miall, A.D., 1985b, Sedimentation on an early Proterozoic continental margin under glacial influence: the Gowganda Formation (Huronian), Elliot Lake area, Ontario, Canada: *Sedimentology*, v. 32, p. 763–788.
- Miall, A.D., 2006, *The geology of fluvial deposits*: Springer, 599 p.
- Miller, K.G., Kominz, M.A., Browning, J. V., Wright, J.D., Mountain, G.S., Katz, M.E., Sugarman, P.J., Cramer, B.S., Christie-Blick, N., and Pekar, S.F., 2005, The Phanerozoic record of global sea-level change: *Science (New York, N.Y.)*, v. 310, p. 1293–1298, doi: 10.1126/science.1116412.
- Mossop, G.D., and Flach, P.D., 1983, Deep channel sedimentation in the Lower Cretaceous McMurray Formation, Athabasca Oil Sands, Alberta: *Sedimentology*, v. 30, p. 493–509, doi: 10.1111/j.1365-3091.1983.tb00688.x.
- de Mowbray, T., 1983, The genesis of lateral accretion deposits in recent intertidal mudflat channels, Solway Firth: *Sedimentology*, v. 30, p. 425–435, doi: 10.1111/j.1365-3091.1983.tb00681.x.
- Mulhern, J.S., Johnson, C.L., Stright, L.E., and Chentnik, B.M., 2014, Implications of an expanded section and delta deposits in the Cretaceous Straight Cliffs Formation in

the northern Kaiparowits Plateau, southern Utah, USA, *in* Abstracts with Program: AAPG Annual Convention and Exhibition 2014, Houston, TX,.

- Musial, G., Reynaud, J.Y., Gingras, M.K., Féliès, H., Labourdette, R., and Parize, O., 2012, Subsurface and outcrop characterization of large tidally influenced point bars of the Cretaceous McMurray Formation (Alberta, Canada): *Sedimentary Geology*, v. 279, p. 156–172, doi: 10.1016/j.sedgeo.2011.04.020.
- Nardin, T.R., Feldman, H.R., and Carter, B.J., 2013, Stratigraphic architecture of a large-scale point-bar complex in the McMurray Formation: Syncrude's Mildred Lake Mine, Alberta, Canada, *in* Hein, F.J., Leckie, D., Larter, S., and Suter, J.R. eds., Heavy-oil and oil-sand petroleum systems in Alberta and beyond: AAPG Studies in Geology 64, p. 273–311.
- Nichol, S.L., Zaitlin, B.A., and Thom, B.G., 1997, The upper Hawkesbury River, New South Wales, Australia: a Holocene example of an estuarine bayhead delta: *Sedimentology*, v. 44, p. 263–286, doi: 10.1111/j.1365-3091.1997.tb01524.x.
- Olariu, C., and Bhattacharya, J.P., 2006, Terminal distributary channels and delta front architecture of river-dominated delta systems: *Journal of Sedimentary Research*, v. 76, p. 212–233, doi: 10.2110/jsr.2006.026.
- Page, K.J., Nanson, G.C., and Frazier, P.S., 2003, Floodplain formation and sediment stratigraphy resulting from oblique accretion on the Murrumbidgee River, Australia: *Journal of Sedimentary Research*, v. 73, p. 5–14, doi: 10.1306/070102730005.
- Painter, C.S., and Carrapa, B., 2013, Flexural versus dynamic processes of subsidence in the North American Cordillera foreland basin: *Geophysical Research Letters*, v. 40, p. 4249–4253, doi: 10.1002/grl.50831.
- Peterson, F., 1969a, Cretaceous sedimentation and tectonism in the southern Kaiparowits Region, Utah. USGS Open File Report 1314, Sequence Stratigraphy and Basin Evolution of the Kaiparowits Plateau: 272 p.
- Peterson, F., 1969b, Four new members of the Upper Cretaceous Straight Cliffs Formation in the southeastern Kaiparowits Region, Kane County, Utah: *Geological Survey Bulletin*, p. J1–J28.
- Pettinga, L.A., 2013, Tectonic controls on alluvial architecture in the Upper Cretaceous John Henry Member, Straight Cliffs Formation, southern Utah: The University of Utah, 300 p.
- Plink-Björklund, P., 2008, Wave-to-tide facies change in a campanian shoreline complex, Chimney Rock Tongue, Wyoming-Utah, U.S.A: *SEPM Special Publication*, v. 90, p. 265–291.
- Pranter, M.J., Hewlett, A.C., Cole, R.D., Wang, H., and Gilman, J., 2013, Fluvial architecture and connectivity of the Williams Fork Formation: use of outcrop analogues for stratigraphic characterization and reservoir modelling, *in* Sediment-Body Geometry and Heterogeneity: Analogue Studies for Modelling the Subsurface, Geological Society of London Special Publication, p. 57–83.

- Rahmani, R.A., 1989, Cretaceous tidal estuarine and deltaic deposits, Drumheller, Alberta. Canadian Society of Petroleum Geologists, Field Guide to: Second International Research Symposium on Clastic Tidal Deposits, August 22-25, Calgary, Alberta: 59 p.
- Rahmani, R.A., 1988, Estuarine tidal channel and nearshore sedimentation of a Late Cretaceous Epicontinental Sea, Drumheller, Alberta, Canada, *in* de Boer, E.L., van Gelder, A., and Nio, S.D. eds., *Tide-Influenced Sedimentary Environments and Facies*, p. 433–471.
- Reynolds, T., 2005, Paralic oil and gas fields. What makes them distinctive: from the pore scale to the reservoir scale, *in* AAPG Distinguished Lecture.
- Rodriguez, A.B., Simms, A.R., and Anderson, J.B., 2010, Bay-head deltas across the northern Gulf of Mexico back step in response to the 8.2ka cooling event: *Quaternary Science Reviews*, v. 29, p. 3983–3993, doi: 10.1016/j.quascirev.2010.10.004.
- Roy, P.S., 1994, Holocene estuary evolution- stratigraphic studies from southeastern Australia, *in* Dalrymple, R.W. and Boyd, R.L. eds., *Incised Valley Systems: Origin and Sedimentary Facies*, SEPM Special Publication, p. 241–263.
- Schellenbach, W.L., 2013, Sequence stratigraphy of an ancient fluvial megafan: Drip Tank Member of the Straight Cliffs Formation (Late Cretaceous), Southern Utah, USA: Department of Geology and Geophysics, 148 p.
- Shanley, K.W., and McCabe, P.J., 1991, Predicting facies architecture through sequence stratigraphy-an example from the Kaiparowits Plateau, Utah: *Geology*, v. 19, p. 742–745, doi: 10.1130/0091-7613(1991)019<0742:PFATSS>2.3.CO;2.
- Shanley, K.W., McCabe, P.J., and Hettlinger, R.D., 1992, Tidal influence in Cretaceous fluvial strata from Utah, USA: a key to sequence stratigraphic interpretation: *Sedimentology*, v. 39, p. 905–930, doi: 10.1111/j.1365-3091.1992.tb02159.x.
- Simms, A.R., and Rodriguez, A.B., 2014, The influence of valley morphology on the rate of bayhead delta progradation: *Journal of Sedimentary Research*, v. 85, p. 38–44, doi: 10.2110/jsr.2015.02.
- Smith, D.G., Hubbard, S.M., Leckie, D.A., and Fustic, M., 2009, Counter point bar deposits: lithofacies and reservoir significance in the meandering modern peace river and ancient McMurray formation, Alberta, Canada: *Sedimentology*, v. 56, p. 1655–1669, doi: 10.1111/j.1365-3091.2009.01050.x.
- Stanley, K.O., and Surdam, R.C., 1978, Sedimentation on the front of Eocene Gilbert-type deltas, Washakie Basin, Wyoming: *Journal of Sedimentary Petrology*, v. 48, p. 557–573, doi: 10.1306/212F74D2-2B24-11D7-8648000102C1865D.
- Steel, R.J., Plink-Bjorklund, P., and Aschoff, J., 2012, Tidal deposits of the Campanian Western Interior Seaway, Wyoming, Utah and Colorado, USA, *in* Davis, R.A. and Dalrymple, R.W. eds., *Principles of Tidal Sedimentology*, Dordrecht, Springer Netherlands, p. 79–107.

- Strobl, R.S., Muwais, W.K., Wightman, D.M., Cotterill, D.K., and Yuan, L., 1997, Geological modelling of McMurray formation reservoirs based on outcrop and subsurface analogues: Canadian Society of Petroleum Geologists Memoir, v. 18, p. 292–311.
- Suarez, M.B., Gonzalez, L.A., and Ludvigson, G.A., 2010, Estimating the oxygen isotopic composition of equatorial precipitation during the Mid-Cretaceous: Journal of Sedimentary Research, v. 80, p. 480–491, doi: 10.2110/jsr.2010.048.
- Szwarc, T.S., Johnson, C.L., Stright, L.E., and McFarlane, C.M., 2015, Interactions between axial and transverse drainage systems in the Late Cretaceous Cordilleran foreland basin: evidence from detrital zircons in the Straight Cliffs Formation, southern Utah, USA: Geological Society of America Bulletin, v. 127, p. 372–392, doi: 10.1130/B31039.1.
- Tänavsuu-Milkeviciene, K., Plink-Björklund, P., Kirsimäe, K., and Ainsaar, L., 2009, Coeval versus reciprocal mixed carbonate-siliciclastic deposition, Middle Devonian Baltic Basin, Eastern Europe: implications from the regional tectonic development: Sedimentology, v. 56, p. 1250–1274, doi: 10.1111/j.1365-3091.2008.01032.x.
- Terzuoli, A., and Walker, R.G., 1997, Estuarine valley fills in the Lower Cretaceous Bluesky Formation, Edson area, Alberta: Bulletin of Canadian Petroleum Geology, v. 45, p. 194–217.
- Thomas, L., 2012, Coal geology: Wiley-Blackwell, 454 p.
- Thomas, R.G., Smith, D.G., Wood, J.M., Visser, J., Calverley-Range, E.A., and Koster, E.H., 1987, Inclined heterolithic stratification—Terminology, description, interpretation and significance: Sedimentary Geology, v. 53, p. 123–179, doi: 10.1016/S0037-0738(87)80006-4.
- Thornton, R.C.N., 1979, Regional stratigraphic analysis of the Gidgealpa Group, Southern Cooper Basin, Australia: Department of Mines and Energy, Geological Survey of South Australia, 140 p.
- Visser, M.J., 1980, Neap-spring cycles reflected in Holocene subtidal large-scale bedform deposits: a preliminary note: Geology, v. 8, p. 543, doi: 10.1130/0091-7613(1980)8<543:NCRIHS>2.0.CO;2.
- White, C.D., Willis, B.J., and Dutton, S., 2004, Sedimentology, statistics, and flow behavior for a tide-influenced deltaic sandstone, Frontier Formation, Wyoming, United States, in Grammer, G.M., Harris, P.M., and Eberli, G.P. eds., Integration of outcrop and modern analogs in reservoir modeling: AAPG Memoir 80, AAPG, p. 129–152.
- Wightman, D.M., 2003, Oil sands, in Middleton, G.V. ed., Encyclopedia of Sediments and Sedimentary Rocks, Kluwer Academic Publishers, p. 499–502.
- Willis, B., 1997, Architecture of fluvial-dominated valley fill deposits in the Cretaceous Fall River Formation: Sedimentology, v. 44, p. 735–757, doi: 10.1046/j.1365-3091.1997.d01-48.x.

- Willis, B.J., 2005, Deposits of tide-influenced deltas: SEPM Special Publication, v. 83, p. 87–129.
- Willis, B.J., and Gabel, S.L., 2003, Formation of deep incisions into tide-dominated river deltas: implications for the stratigraphy of the Sege Sandstone, Book Cliffs, Utah, U.S.A: *Journal of Sedimentary Research*, v. 73, p. 246–263, doi: 10.1306/090602730246.
- Yang, B.C., Dalrymple, R.W., and Chun, S.S., 2005, Sedimentation on a wave-dominated, open-coast tidal flat, south-western Korea: summer tidal flat - winter shoreface: *Sedimentology*, v. 52, p. 235–252, doi: 10.1111/j.1365-3091.2004.00692.x.
- Yoshida, S., Steel, R.J., and Dalrymple, R.W., 2007, Changes in depositional processes—an ingredient in a new generation of sequence-stratigraphic models: *Journal of Sedimentary Research*, v. 77, p. 447–460, doi: 10.2110/jsr.2007.048.